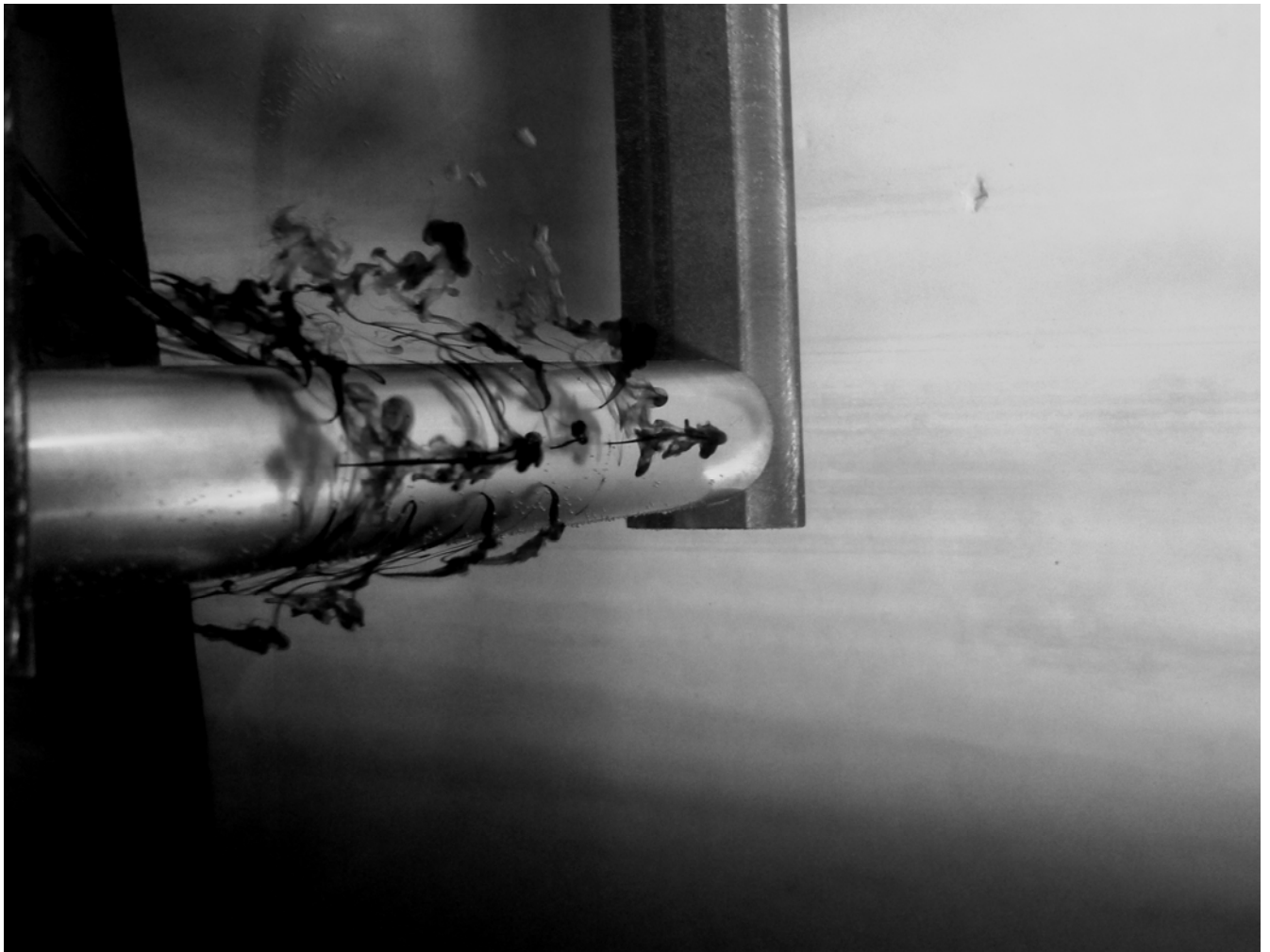


VISUALIZATION AND LDV OF FLOW AROUND A CIRCULAR CYLINDER



ARNAB GANGULY & JEREMY NABETH

**Purdue University
AAE520 - Spring 2009**

ALBUM



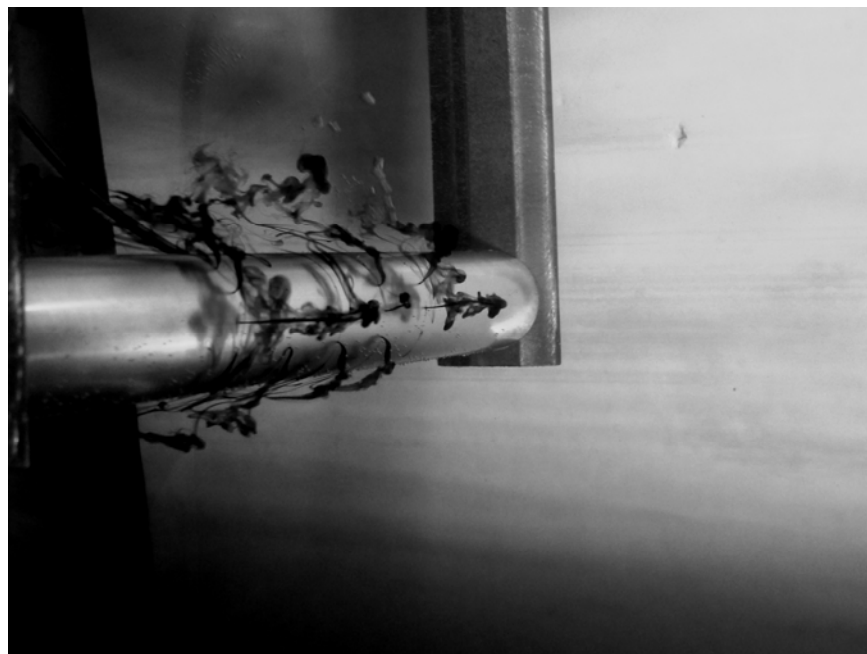
Circular Cylinder at $Re = 900$, at this Reynolds number, transition waves referred to as Gerard-Bloor waves develop along the shear surface. The transition waves are seen as undulations on the shear surface, which then curl up to form eddies. The eddy formation length for this flow configuration was found to be at $\sim 2.8D-2.9D$ from the cylinder. The development of the turbulence can be noticed far downstream (the flow is from right to left)



Circular Cylinder at $Re = 3600$. For the same dye pressure, there was a noticeable increase in the angle at which the free shear layer departs the cylinder surface with reference to the flow direction. It was also noticed that the eddy formation length reduced to ~ 2 times the diameter into the wake. The formation of the turbulent wake can be seen on the left side of the image along with the alternating vortices. However, it was noticed that for the same dye station opening, the water carried a smaller quantity of dye from the dye ports.



Circular Cylinder at $Re= 8100$. At higher Reynolds numbers, the eddy formation length reduces to merely ~ 1.3 times the diameter, bringing the eddies closer to the cylinder surface. As the Reynolds number is increased, the eddies develop in almost fixed locations which then diffuse and decay along their movement downstream. This is accompanied with the shift in the transition region towards the separation point. The formation of the turbulent eddies in the wake can be seen and the lower dye trace in the near wake region develops vortices which are shed with a frequency of ~ 0.8 Hz (detected through a video capture of the dye trace)



This image illustrates the importance of carefully controlling the dye injection flow rate to match the flow velocity. Having a large velocity component of the dye flow perpendicular to the cylinder reduces the accuracy of representation of the flow. In the image above, it is seen that even though the flow is at a $Re \sim 2000$, the near wake suggests the formation of turbulent eddies which is not true for this flow configuration.

TABLE OF CONTENTS

1.ABSTRACT	4
2.LITERATURE REVIEW	4
3.INTRODUCTION	6
4.MOTIVATION	8
5.OBJECTIVES	8
6.BACKGROUND	9
A.FLOW VISUALIZATION	9
B.LASER DOPPLER VELOCIMETRY	10
C.THE WATER TUNNEL	11
D.WAKE BEHIND BLUFF BODIES	12
7.THE EXPERIMENTAL SETUP	13
A.APPROACH	13
B.ANALYSIS OF THE SETUP	18
8.EXPERIMENTAL PROCEDURE	24
9.RESULTS AND DISCUSSION	28
A.CALIBRATION	28
B.FLOW VISUALIZATION	28
C.STATISTICAL ANALYSIS	36
D.WAKE PROFILE	39
E.FLUCTUATIONS	41
10.CONCLUSIONS	46
11.ACKNOWLEDGEMENTS	47
12.REFERENCES	48
13.LIST OF FIGURES	51
14.LIST OF TABLES	53

1. ABSTRACT

The current experimental study involves the use of a low speed water tunnel to analyze the flow around a circular cylinder using dye flow visualization technique. Laser Doppler Velocimetry (LDV), an unobtrusive measuring technique, was used to quantify the flow field characteristics that were observed during flow visualization. The observed dye traces were compared to visualization techniques used earlier and with results of an unsteady simulation of flow around a circular cylinder. The observed angle at which the shear layer departs the cylinder surface and the eddy formation distance, L_f in the wake has been quantified through image processing techniques. A statistical analysis of the flow pattern in the free stream and in the wake has been done. It was observed that the sample frequency of particles followed a near Gaussian distribution in the free stream. Measurements were also made to study the wake profile for different Reynolds numbers and a comparison was made with experimental correlations. Measurements of hot wire anemometry techniques and LDV techniques of the mean wake profile in the wind tunnel and the water tunnel respectively have been compared. It was observed that the measurements made using the LDV technique matched the predicted coefficient of drag for higher Reynolds numbers better than for lower Reynolds numbers. The deviation for a Reynolds number of 5100 was ~6%, while it increased to 15% for Reynolds numbers of ~ 2960. The current work also involves the measurement of the fluctuations for different flow speeds. It was found that the fluctuations in the free stream increased at flow speeds approaching 1 in/s where the fluctuations were found to be at 4%, while that at flow speeds of 10 in/s were at 2% of the mean.

2. LITERATURE REVIEW

Understanding complex flow fields has been aided by the ability to visualize them under a plethora of flow conditions. Water, being denser than air, provides for a convenient medium to visualize the flow field and has thus been extensively used in the past. One of the most important contributions was the use of aniline dye to produce colored water in the Osborne Reynolds experiment conducted in 1883. As the velocity of water was increased in a small tube, the

transition from laminar to turbulent flow was witnessed with the formation of eddies which diffused over time (G.A Tokaty, 1971). The first use of the water tunnel to visualize flow characteristics was made by Ludwig Prandtl where the water was circulated using a paddle wheel driven by hand in 1903. Sandwich electrodes were also used to estimate the flow direction and determine the point of separation in flow over a cylinder placed in a water tunnel (Son, 1968). Reviews of various other experiments and visualizing agents have been covered by (Clayton and Massey, 1967); (Werle, 1973); (Merykirch, 1974); and (Erickson, 1981). The most significant development in the field of dye flow visualization began with ONERA in France, with the work of (Werley, 1973) and Roy conducted in the early 1950s. The flow visualization carried out at ONERA has been used as a basis for comparison in the present study since it covers the intermediate sub critical flow regime. A large number of dyes have been used for marking of streak lines (Merykirch, 1974). Some of the popularly used dyes are milk, food coloring and inks. Use of fluorescent materials have also been discussed by (Beckner and Curry 1985) and (Campbell, 1973). It was found that the stability of the dye traces improved with the use of milk in small concentrations along with the dye. The fat content was believed to have retarded the diffusion. The basic requirement from the dye flow visualization techniques is that the dye traces must follow the fluid path and must be introduced at the same velocity as that of the fluid being analyzed. Different methods are adopted to inject the dye in the flow. One such technique involves the use of a dye probe. It makes use of a hypodermic needle to inject the dye in the flow. The biggest advantage of using the technique is that it provides for easy means of varying the location at which the dye is released. On the other hand, the disadvantage is that, it disturbs the flow field. To circumvent this problem, we decided to use dye ports that were an integral part of the model itself. In this technique, it is important to ensure that the component of the velocity of the dye perpendicular to the model surface is small. The visualization was carried out with the help of the dye that was available in Lab 3.

The use of LDV for quantifying the fluid velocities was first introduced by (Cummins, Knable and Yeh, 1964) where the Brownian motion of particles was studied by analyzing micron sized particles in the flow. Thereafter, the experiment conducted by (Yeh and Cummins, 1964) demonstrated the use of the LDV in making velocity measurements. Successful measurements were made of laminar flow in a square duct by (Kreid, 1966) and (Goldstein, 1967) and in a circular duct by (Foreman, 1966), laminar gas flows by (James, 1967) and turbulent flow in pipes

by (Goldstein and Hagen, 1967). The LDV technique was chosen in the current study to overcome the limitations of using a hot wire. A hot wire disturbs the flow, moreover, it imposes limitations on the location of the probe for taking measurements.

Flow characteristics around a circular cylinder have received much attention from researchers in the past. These include (Roshko, 1961); (Tani 1964, 1967); (Jones Cincotta and Walker, 1969); (Achenbach 1968, 1971, 1977); (Szechenyi, 1975); (Guven, Patel and Farell, 1977); (Guven, Farell and Patel, 1980) and (Farell 1981). Use of dye injection techniques to study the variations along the span-wise direction of cylinders were previously done by (Hama, 1957) and (Gerrard, 1978). However, the interpretations of flow fields characterized by dye traces require some careful considerations which have been discussed by (Hama, 1962). CR Smith at Lehigh University examined the wake of a cylinder for variations along the span-wise direction. With the aid of dye flow visualization, the current study is intended to help understand some of the characteristics that govern the flow field around a circular cylinder. It would also include a systematic analysis of the fluctuations in the velocity of the fluid particles in the wake of a circular cylinder. A comparison will also be made between the use of LDV techniques and hot wire probes in making velocity measurements.

3. INTRODUCTION

Water Tunnels have played an important role in understanding complex flows dominated by vortices and vortex interactions. Flow visualization in water tunnels provide an excellent means to observe the flow for a wide variety of flow configurations. The use of fluorescent dyes in 3D imaging was explained by (Hoffmann et al, 2005) , their use in engine intake flows was explained by (Węclaś, M et al,1993); shear layer injection methods were investigated by (Shen and Gongxin, 1992) and the determination of the geometric position of vortices in flow fields was studied by (Foerster S, 1989). Flow around a circular cylinder forms the basis for the understanding of the classical flow around a bluff body, a subject that has several practical applications.

The effect of Reynolds number has been singled out as the governing parameter and the start/end of a flow regime may be specified by a set of Reynolds numbers. At Reynolds numbers of 0.2, we expect no separation; the shear layers do not form a visible wake. In the flow regime between

$0 < Re < 200$, the state of flow is divided into 3 distinct sub-regimes, creeping flows for $Re < 4$, closed near-wake regime for $Re < 50$ and periodic laminar regime for $Re < 200$. At Reynolds numbers $= 5$, we expect a steady separation bubble, but no Karman Vortices. Separation is initiated at $Re \sim 6$, with the formation of a visible symmetric wake. For $Re > 45$, the closed near wake becomes unstable and a sinusoidal oscillation of the wake commences. At Reynolds numbers > 100 , we expect to see Von Karman vortices being shed but no turbulence in the boundary and shear layers. At Re of ~ 200 , the wake becomes unsteady and turbulence sets in further downstream. Increasing the Re further, the turbulence moves upstream. Between $200 < Re < 400$, there is a phase at which the vortex shedding frequency changes, indicating a shift from laminar eddies to irregular eddies. For Re varying between 400 and 2000, development of transition waves commences with the onset of transition in the shear layers. With the current setup, we expect to reach Reynolds numbers of $\sim 10,000$. The diameter of the cylinder was restricted to 1.5in since it provided the maximum overlap between the Reynolds numbers achieved by the wind tunnel and that in the water tunnel. At the same time, in order to make an accurate comparison, it was necessary to take the measurements in the wake such that the distances at which the wake profiles were measured in the two tunnels were the same. The measurements in the wind tunnel being made at 7.5 times the diameter of the cylinder, it was necessary to maintain the same for measurements in the water tunnel. With a 1.5in cylinder in the water tunnel, this occurs at the end of the test section. Thus it was not possible to increase the Reynolds number range any further for the same downstream distance as that used in the wind tunnel. The following section contains the motivation and objectives of the current study.

Reynolds Number Range	Flow Characteristics
$Re < 0.2$	No Separation
$Re < 4$	Creeping flows
$Re < 50$	Closed near-wake, steady separation bubble
$Re < 200$	Unsteady wake- referred to as periodic laminar
$200 < Re < 400$	Change in the vortex shedding frequency
$400 < Re < 10000$	Onset of transition in the shear layers and turbulent wake

Table 1: Flow Regimes

4. MOTIVATION

Analysis of the wake profile using a hot wire probe provided useful insights into the wake characteristics of a cylinder. However, since we used a wind tunnel which was not provided with flow visualization capabilities, we tried visualizing the flow field using computational techniques. An attempt was made at visualizing the flow around a cylinder using the sting made to support the cone in Lab 3. Figure 1 represents the flow as it developed by placing the dye tube upstream from the sting in Lab 3, clearly indicating the fact that the dye did not take up the path of the flow. Unable to find an effective means of injecting the dye, we were keen on setting up a means to visualize the flow around a cylinder.

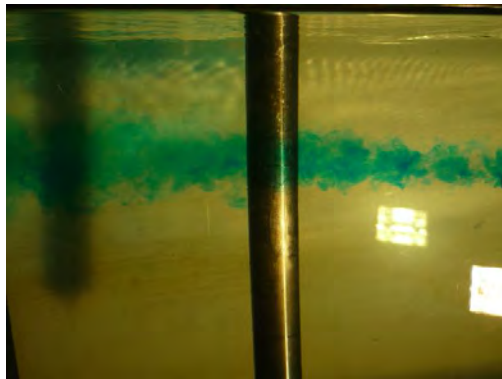


Figure 1: Flow Visualization around the Sting in Lab

5. OBJECTIVES

- Design a setup which will help us visualize the flow over a cylinder across a wide range of Reynolds number (up to $Re = 10,000$)
- To bridge the gap that exists between Lab 1 and Lab 3 in such a way that data quantified in Lab 1 using a hot wire probe can be visualized in the water tunnel and also sets up a means of comparing measurements using the hot wire probe and LDV techniques.
- To determine whether there is accurate scaling of flow parameters between the use of air and water as the fluid medium

6. BACKGROUND

a. Flow Visualization

Flow visualization involves the study of methods to display dynamic behavior in liquids and gases and making these patterns visible. In experimental fluid dynamics, flows can broadly be visualized using three methods: surface flow visualization techniques, particle/molecule tracer methods and optical methods. Surface flow visualization reveals the flow streamlines in the limit as a solid surface is approached. Colored oil applied to the surface of a wind tunnel model provides one such technique (Smits, A.J and Lim T.T, 2000). Particles, such as smoke, can be added to a flow to trace fluid motion. Illuminating the particles in a fluid with a sheet of laser light has been used extensively in order to visualize a complicated flow field. Laboratory flow visualization has become more exact, with careful control of the particulate size and distribution. Advances in photography have also helped in extending our understanding of various flow fields.

The observations of fluid motion using smoke and dye is one of the oldest. The technique is relatively inexpensive. Food dyes are used as a means of visualizing the flow. Colors that are generally used include red, blue and green due to their ability to provide a good contrast. In general, the dyes that are available have a specific gravity greater than that of water. Thus, in order for it to be neutrally buoyant when used in a water tunnel, it needs to be diluted with a small amount of alcohol, such as methanol or ethanol. Further, to ensure that the dye and the fluid medium are at a minimum temperature differential, the dye is diluted with the fluid comprising the flow field. The extent of dilution is a trade-off between good visual effects and that of incorrect flow field representation.

It is however not sufficient just to visualize the flow field. Attributing flow characteristics requires quantifying the observations in the flow field. One technique used to quantify the observations involves estimating the flow velocity of particles by the use of a laser beam. This can be done using laser doppler velocimetry (LDV).

b. Laser Doppler Velocimetry

The LDV crosses two beams of collimated, monochromatic and coherent laser light in the flow field of interest. The two beams are obtained by splitting a single beam, thus ensuring good coherence. According to the Doppler effect, the change in wavelength of the reflected radiation is a function of the targeted object's relative velocity, which in this case refers to a particular particle in the fluid. Particles moving through the fringes scatter light whose intensity fluctuates with a frequency that is related to the particles velocity. Thus, the velocity of the particle can be obtained by measuring the change in wavelength of the reflected laser light, which is done by forming an interference fringe pattern referred to as the Young's interference fringes, as shown in Figure 2.

These variations are monitored using a Tektronix Oscilloscope. The intensity variations are then converted to FFT's from which the peak intensity corresponding to the frequency associated with a unique particle is analyzed to obtain the velocity of the particle in the flow. The LDV thus gives an accurate, non-intrusive method for measuring absolute velocity of a particle in the flow. The frequency (f) of the interference signal output to the oscilloscope can be used to find the velocity (v) of a particle impinging on the crossed laser using the wavelength of the laser light (λ) and the angle (θ) between the crossed beams as given by the equations below; Here S corresponds to the time period of the oscillating signal.

$$S = \frac{\lambda}{2 \sin\left(\frac{\theta}{2}\right)}$$
$$V = fS = \frac{f\lambda}{2 \sin\left(\frac{\theta}{2}\right)}$$

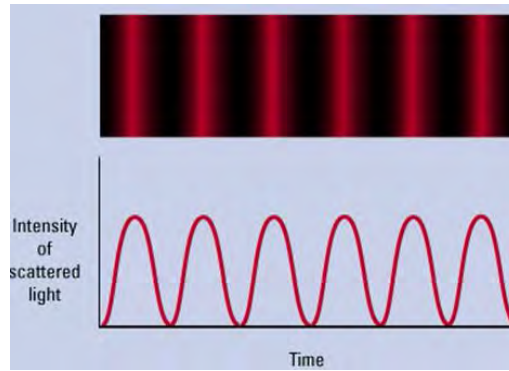


Figure 2: Fringe Pattern obtained by the interference of two coherent laser beams and the resulting intensity distribution

c. The Water Tunnel

A water tunnel provides a convenient means of visualizing the flow field around an object. The properties of water make it a preferred means of flow visualization compared to tunnels using air. It provides for the usage of dyes which are easier to visualize compared to the usage of an MTV technique which would require the use of a tagging molecule and subsequent fluorescence or phosphorescence. It can also be used to obtain 2D images by passing a sheet of a high intensity laser beam across the model. Seeding the flow with fluorescent dyes or particles can enhance the quality of the images that are captured and the subsequent quantitative analysis that is carried out.

The tunnel used for the purpose of the experiment was a closed circuit water tunnel oriented horizontally and accessible from the top. The presence of good optical access from a section on either side of the tunnel and one along the downstream section of the tunnel provided for good 3D flow visualization. The test section measured 15''x 20''x 64''. A schematic of the tunnel is provided in Figure 3, (Eidetics International Inc., 2004). The flow of water in the tunnel reaches a maximum of 900 gallons/min providing a velocity of a foot per second. The flow is made to pass through a perforated cylinder which reduces the turbulence in the water. The flow is controlled by means of a centrifugal pump driven by a 15HP electric motor. The dye supply system was provided with multiple dye stations. The supply system was pressure controlled to facilitate accurate control of the dye injection. Means were provided for blowing air out of the dye lines. The dye canisters were pressurized with the help of a compressor to provide for the required air pressure. The pressure was monitored using a regulator provided along the supply line.

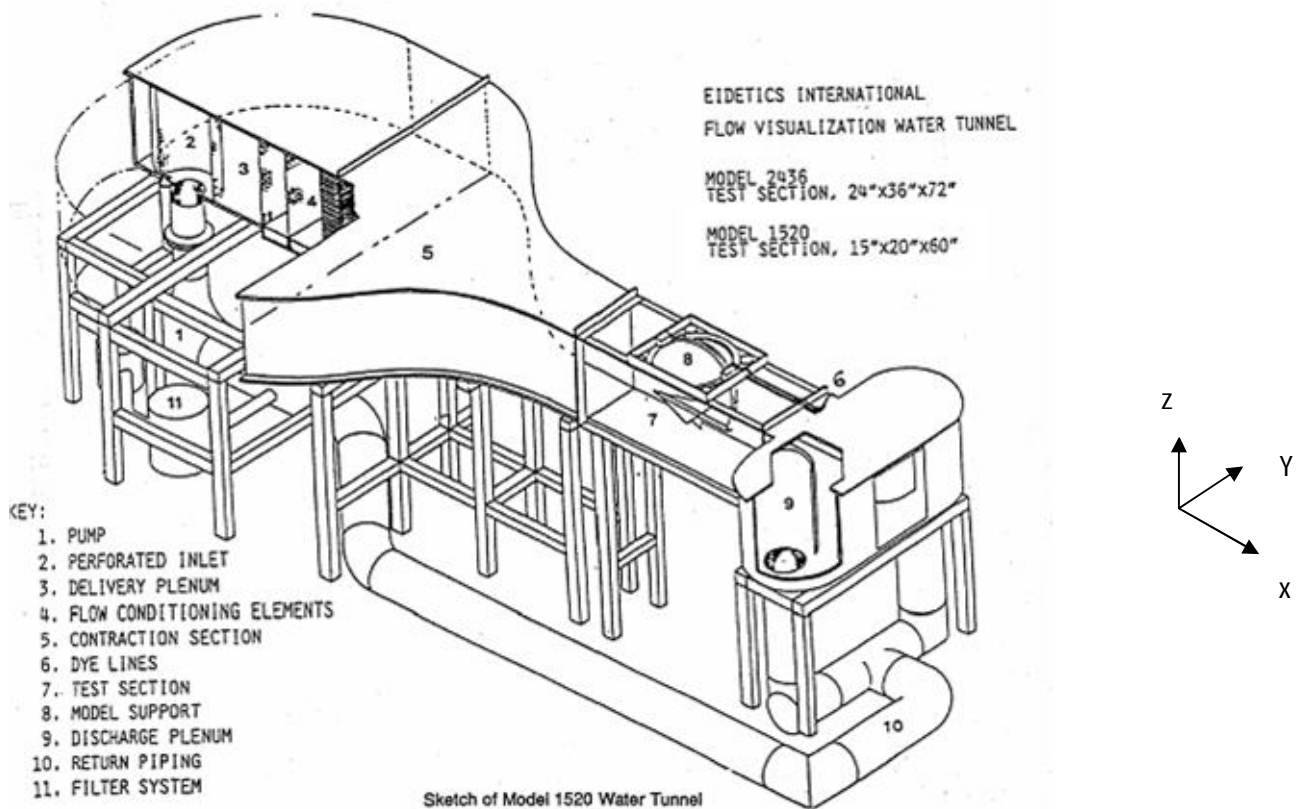


Figure 3: Schematic of the water tunnel

d. Wake Behind Bluff Bodies

Consider a flow field consisting of a fluid flowing around a cylinder at a Reynolds number greater than 1. The pressure reaches a maximum at the stagnation point and gradually decreases on either side of the front half of the cylinder. The flow stays attached in this region characterized by a favorable pressure gradient. Beyond that, the pressure starts to increase and the flow begins to experience an adverse pressure gradient. Consequently, the flow separates from the surface, creating a highly turbulent region behind the cylinder called the wake. The boundary layer that separates is highly unstable. This eventually forms a vortex and detaches itself from the surface. They are shed alternately from the cylinder and generate a regular vortex pattern, referred to as the Von Karman vortex street. The frequency with which the vortices are shed can be quantified with the non-dimensional Strouhal number, S . This number is given by

$$S = df/U_{\infty}$$

where d is the diameter of the cylinder, f is the shedding frequency, and U_∞ is the free stream velocity.

Bluff bodies are generally associated with large velocity deficits in the wake which in turn lead to high drag forces on them. The wake grows downstream and is governed by a self similar solution. Figure 4 shows the drag coefficient for a smooth cylinder as a function of Reynolds number, (Schlichting, 1979).

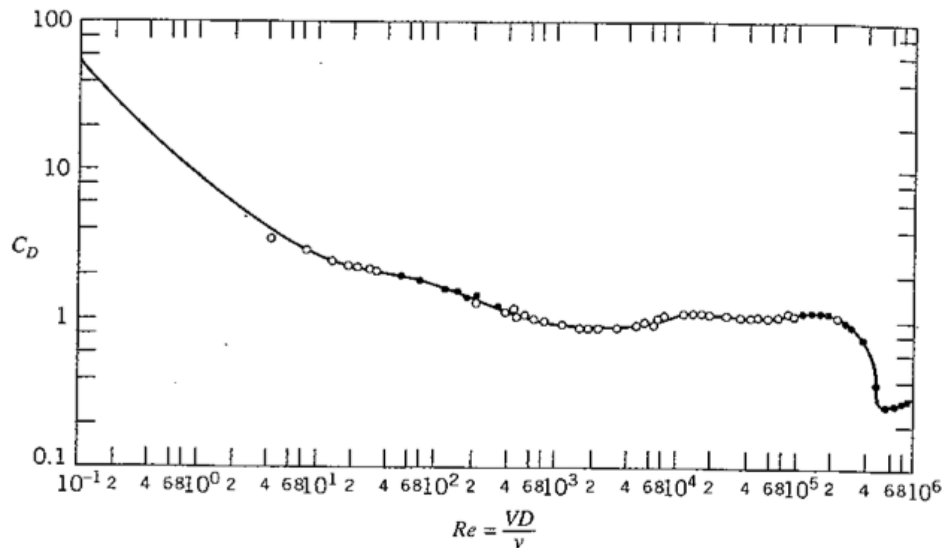


Figure 4: Drag Coefficient for a smooth cylinder as a function of Reynolds number

7. THE EXPERIMENTAL SETUP

a. Approach

With the goal of designing an experimental setup that could be re-used in the future, the primary aim was to design a structure that would be light and easy to set up. The model was needed to visualize and measure the flow characteristics around a cylinder. Since the measurements were to be done using Laser Doppler Velocimetry, we had to adapt our design so as to capitalize on the improved resolution of the probe volume in the y direction. We knew that the two lasers cross, maintaining a width of 1.3 cm along the horizontal axis, so we decided to place the cylinder horizontally. Also, in order to reduce surface effects, we had to position the cylinder half way into the water tunnel from the top surface and also reduce the disturbances generated by our structure in the flow. Considering the machining costs involved, we needed to

design a structure that was easy and quick to machine. A view of the assembly is shown in Figure 5, a discussion of each of the parts follows.

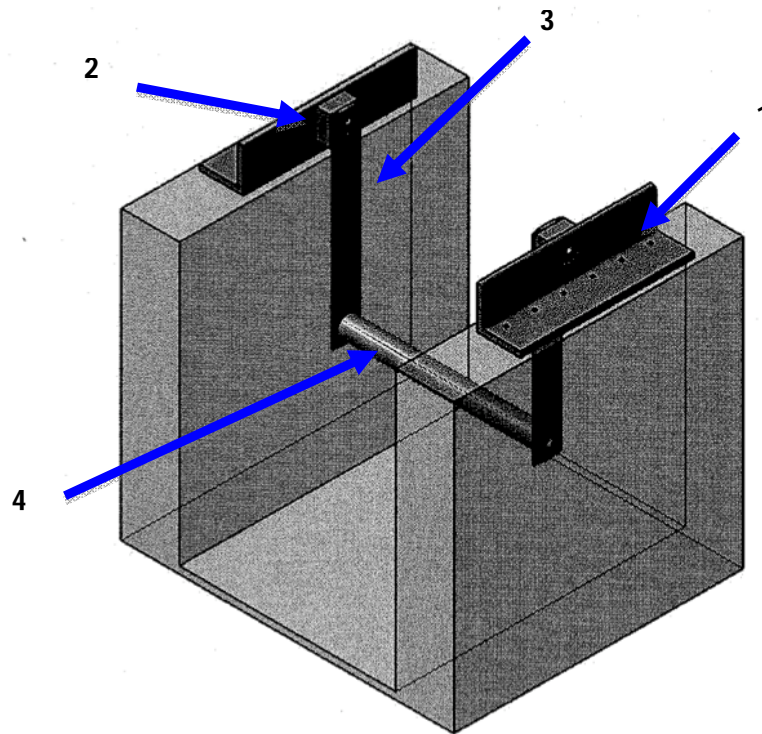


Figure 5: Isometric view of the assembly

1. L plates

The L plates were modeled based on the ones used for the nose cone in the third lab. Figure 6 represents the sectional view of the L plate (part 1). The 0.5 in diameter holes on the front face were provided to mount the plate on the water tunnel while the 0.25 in holes were provided to accommodate angular positioning of the model. The holes visible in the sectional view B-B were provided to arrest the rotary motion when the tunnel is in operation.

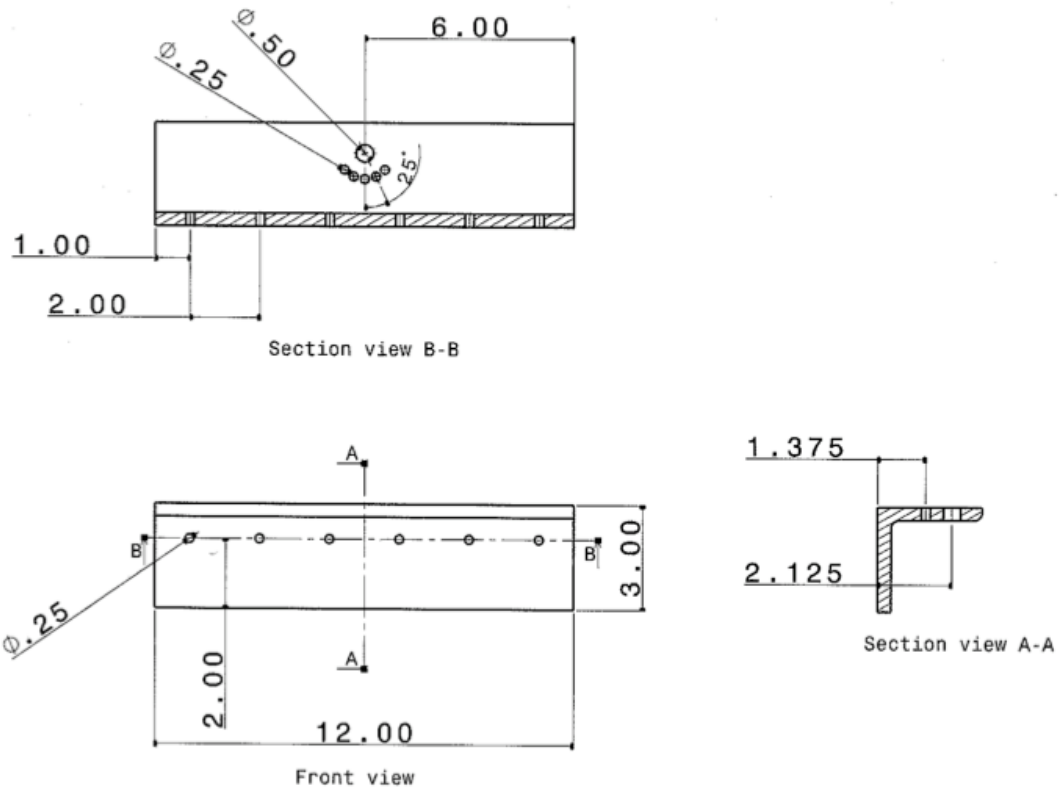


Figure 6: Sectional view of the L Plate

2. Spacers

Part 2 in Figure 5 represents the spacers used. They were incorporated in the design with the objective of providing sufficient tolerance between the struts and the glass of the tunnel

3. Struts

The struts (part 3) in Figure 5, supports the cylinder in the tunnel and prevent it from translational or rotary movement during operation. They are provided with two holes at its upper end which are used to mount them onto the L-plates through the spacers. It was extremely important to design the struts in such a way that its thickness was small and did not extend beyond the cylinder diameter significantly. A larger strut would block the path of the laser, preventing measurements close to the cylinder surface. In order to reduce the disturbance caused in the flow, the leading and trailing edges of the strut were symmetrically chamfered.

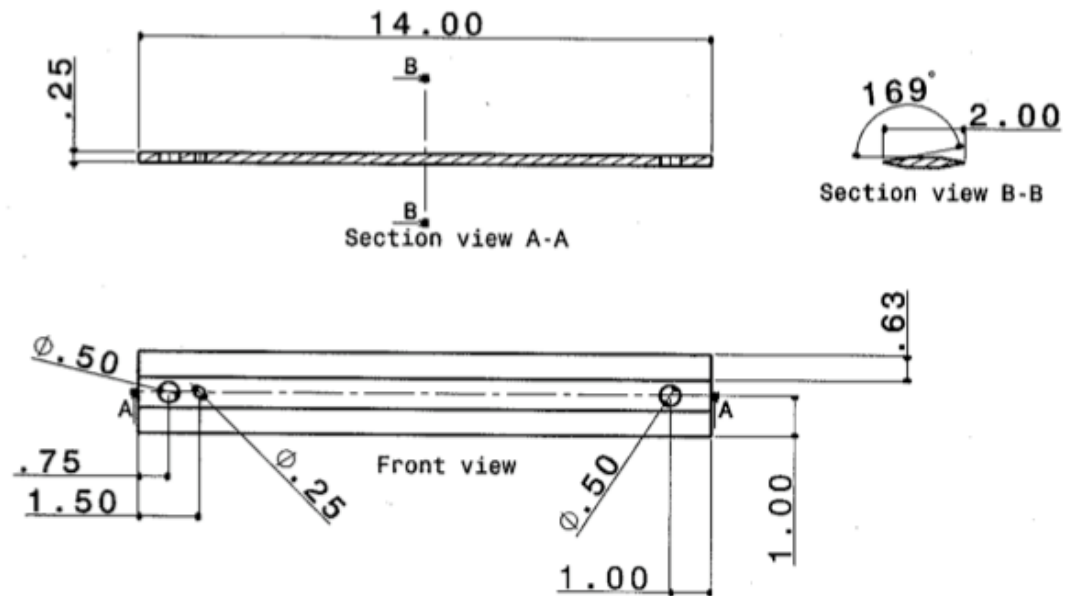


Figure 7: Sectional view of the struts

4. Cylinder

The choice of the cylinder was based on two prerequisites. Firstly, we wanted to reach a wide range of Reynolds numbers, knowing that the flow speed in the water tunnel goes from 1 in/s to 12 in/s. Secondly, in order to compare LDV measurements in the water tunnel with the hot wire anemometer in the wind tunnel, we needed to make measurements at the same distance in the wake. While the closest distance was fixed in the wind tunnel to 7.5 D where D is the diameter of the cylinder, the maximum distance available for measurements in the water tunnel was ~15 in, restricting the largest diameter for a comparison between the two techniques. We used a cylinder with a diameter of 1.50 in, allowing us to make measurements for a range of Reynolds numbers from 900 to 9000.

The cylinder is shown in Figure 8. The 0.50 in diameter hole running through the axis of the cylinder passes dye into the dye ports, each of diameter 0.0 25 in. The dye ports are separated by 25 degrees on the side that faces the flow; provided with 5 such dye stations. This is done to improve the visualization of the streamlines in the boundary layer and avoid the injection of dye directly into the wake. The cylinder was to be fixed onto the struts with the help of two stainless steel flat head screws

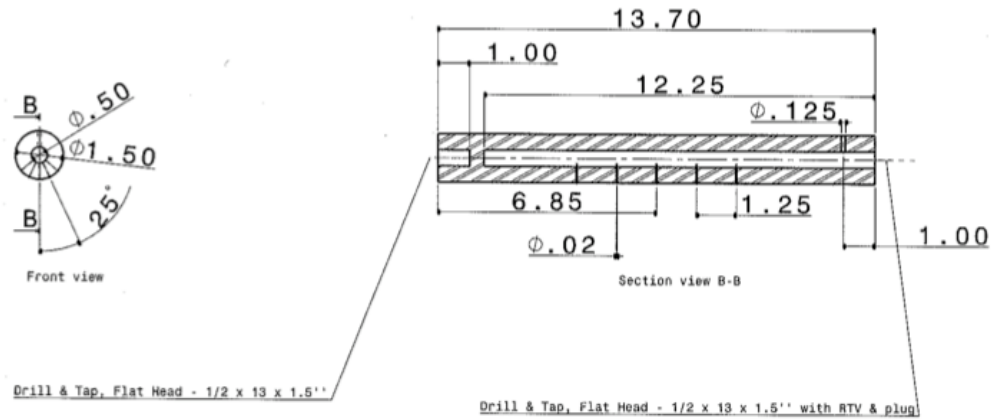


Figure 8: Sectional view of the cylinder

Part Name		Material	Total number to be made	Availability
Spacer Block		Aluminum	2	Available in the Machine Shop
Angle Plate		Aluminum	2	To be ordered
Strut		Stainless Steel 303	2	To be ordered
Cylinder		Aluminum	1	To be ordered
Tubing for the dye		Brass	1	Available in the Machine Shop
Fastener:	1/2x13x3	Stainless Steel	2	Available in the Machine Shop
	1/4x20x3	Stainless Steel	2	Available in the Machine Shop
	1/2x13x1.5	Stainless Steel	2	Available in the Machine Shop

Table 2: Description of each of the Parts for the Setup along with the Required Quantity

b. Analysis of the Setup

In order to analyze the structural integrity of the setup, we carried out an FEM analysis in CATIA. The following section discusses some of the details. The setup was found to have a total mass of ~4 kg which aligned itself well with the objective of designing a light setup. The details of the analysis on each of the parts are shown in Figures 9-12.

Characteristics		Inertia center	
Volume:	4.103e-004m ³	x:	730.035mm
Mass:	1.112kg	y:	-349.426mm
Surface:	0.095m ²	z:	235.082mm
Inertia matrix			
Ixx:	0.001kgxm ²	Ixy:	0kgxm ²
Iyx:	0kgxm ²	Iyy:	0.009kgxm ²
Izx:	0kgxm ²	Izy:	-3.457e-004kgxm ²
		Izz:	0.009kgxm ²

Figure 9: Mechanical characteristics of the Angle Plate

Characteristics		Inertia center	
Volume:	6.153e-005m ³	x:	730.035mm
Mass:	0.167kg	y:	-314.06mm
Surface:	0.012m ²	z:	260.481mm
Inertia matrix			
Ixx:	4.636e-005kgxm ²	Ixy:	0kgxm ²
Iyx:	0kgxm ²	Iyy:	7.551e-005kgxm ²
Izx:	0kgxm ²	Izy:	0kgxm ²
		Izz:	4.707e-005kgxm ²

Figure 10: Mechanical characteristics of the Spacer Block

Characteristics		Inertia center	
Volume:	7.806e-005m ³	x:	730.035mm
Mass:	0.212kg	y:	56.145mm
Surface:	0.037m ²	z:	107.821mm
Inertia matrix			
Ixx:	0.002kgxm ²	Ixy:	0kgxm ²
Iyx:	0kgxm ²	Iyy:	0.002kgxm ²
Izx:	0kgxm ²	Izy:	0kgxm ²
		Izz:	2.785e-005kgxm ²

Figure 11: Mechanical characteristics of the Strut

Characteristics		Inertia center	
Volume:	3.539e-004m ³	x:	730.036mm
Mass:	0.959kg	y:	-120.393mm
Surface:	0.058m ²	z:	-44.153mm
Inertia matrix			
Ixx:	0.01kgxm ²	Ixy:	5.15e-007kgxm ²
Iyx:	5.15e-007kgxm ²	Iyy:	1.927e-004kgxm ²
Ixz:	6.939e-018kgxm ²	Izy:	0kgxm ²
		Izz:	0.01kgxm ²

Figure 12: Mechanical characteristics of the Cylinder

1. The Mesh

The strut being the critical component of the setup has been analyzed for structural integrity and the details, discussed in this section. The mesh used for the analysis had parabolic elements, with a characteristic size of 3 mm and absolute sag of 0.3 mm. Ideally, the characteristic size should corresponds to the smallest dimension on the structure and the absolute sag is commonly chosen as 1/10 of the characteristic size; but in our case the smallest dimension is characterized by the size of the chamfers (0.174mm) which led to virtual memory problems. We thus analyzed the structure based on the width of the strut, we decided to divide this size by two and use it as the characteristic dimension. Figure 13 gives details about the quality of the mesh.

Entity		Size
Nodes		39343
Elements		22226

Connectivity	Statistics
TE10	22226 (100.00%)

Criterion	Good	Poor	Bad	Worst	Average
Stretch	21377 (96.18%)	849 (3.82%)	0 (0.00%)	0.112	0.613
Aspect Ratio	21976 (98.88%)	146 (0.66%)	104 (0.47%)	17.259	1.965

Figure 13: Mesh characteristics

As we can see from the Element Quality table, 0% of our elements have a bad stretch and only 0.47% have a bad aspect ratio. The stretch is poor for 3.82% of the elements and the aspect ratio is poor for 0.66% of our elements. The mesh quality was thus acceptable for more than 96% of the elements.

2. Inputs

The mesh having been chosen, we needed to specify the inputs for the calculations. The holes provided to mount the strut to the spacers were set for zero degrees of freedom. The relevant force that would act on the component was the force due to the flow over the cylinder that has an effect on the strut on account of the cylinder being fixed to the struts.

In order to find the value of this force, we applied Bernoulli's theorem on a streamline that moves from upstream to the stagnation point of the cylinder, assuming that the flow is steady, irrotational, incompressible and laminar, we get:

$$P_a + \frac{1}{2} \rho v_a^2 + \rho g z_a = P_b + \frac{1}{2} \rho v_b^2 + \rho g z_b$$

Where P_a , V_a and Z_a are the Pressure, velocity and height of a particle upstream and P_b , V_b and Z_b are the characteristics from a particle at the stagnation point. We assume uniform flow, so we can state that on the streamline $Z_a = Z_b$; and since the point B is at the stagnation point, we have $V_b = 0$. So the equation becomes:

$$P_b = P_a + \frac{1}{2} \rho v_a^2$$

If we consider a frame that moves with the flow, we can state that the flow is steady and therefore applying Bernoulli's theorem between one point at the free surface and the point A, We have:

$$P_0 + \frac{1}{2} \rho v_0^2 + \rho g z_0 = P_a + \frac{1}{2} \rho v_a^2 + \rho g z_a$$

In this case $V_o=V_a=0$ and we obtain:

$$P_a = P_0 + \rho g(z_0 - z_a)$$

Thus, we have:

$$P_b = P_0 + \rho g(z_0 - z_a) + \frac{1}{2} \rho v_a^2$$

So, with $P_0=1$ atm; $\rho=1000$ kg/(m³); $g=9.81$ m/(s²); $Z_o-Z_a=h=11$ in, and taking the worst case for V_a : $V_a=12$ in/s. We obtain $P_b=104$ MPa.

In order to analyze the worst case possible, we assume the cylinder to be a rectangle with a length and a width equal to that of the cylinder projection ($L=13.70$ in, $W=1.5$ in). And we assume that the pressure is constant across this section. Thus a force of $F_{cyl} = 1.38$ kN acts on the cylinder.

This force will be split between the two struts; so on one strut, we have a force located on the bottom hole of the strut with a value of $F_{cyl} = 0.69$ kN

We also have the effect of the weight of the cylinder on the strut. We know that the mass of the cylinder is equal to 0.959kg,

Once again, this force is split between the two struts, so the value on one strut is 4.7 N

This force will be applied on the bottom hole of the strut, along the y-axis.

Consequently, we have:

$$F_{x \text{ strut}} = -0.69 \text{ kN and } F_{y \text{ strut}} = -4.7 \text{ N}$$

Where F_x and F_y are respectively the components of the force along the x and y directions. The flow of water against the strut applies a pressure and hence a force, which also needs to be accounted for. In order to account for the worst possible case, we considered a uniform pressure equal to that acting at the bottom of the strut (same as that acting on the cylinder).

3. Results

Figure 14 gives the stress computed based on the Von-Mises stress criterion computed by CATIA on the structure. We see that the largest stress is located around the hole of diameter 0.25 in. The largest value was found to be 226 MPa and we know that the material used (Stainless Steel 303) has an elastic modulus of 193×10^3 MPa. Consequently, we can conclude that the design is safe and can withstand the forces in the water tunnel. Figure 15 shows the displacements in the structure, the maximum displacement was found to be 5.34×10^{-2} in, which is small and is not expected to create any significant changes in the flow field.

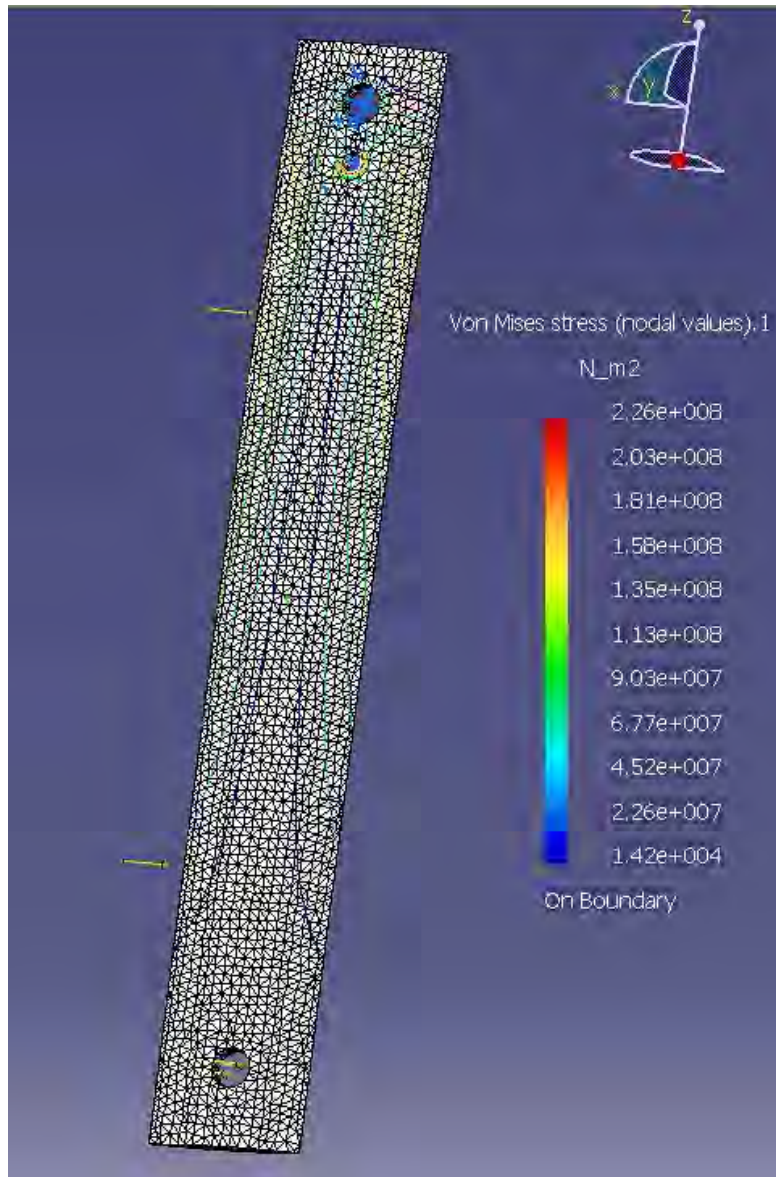


Figure 14: Von Mises Stress

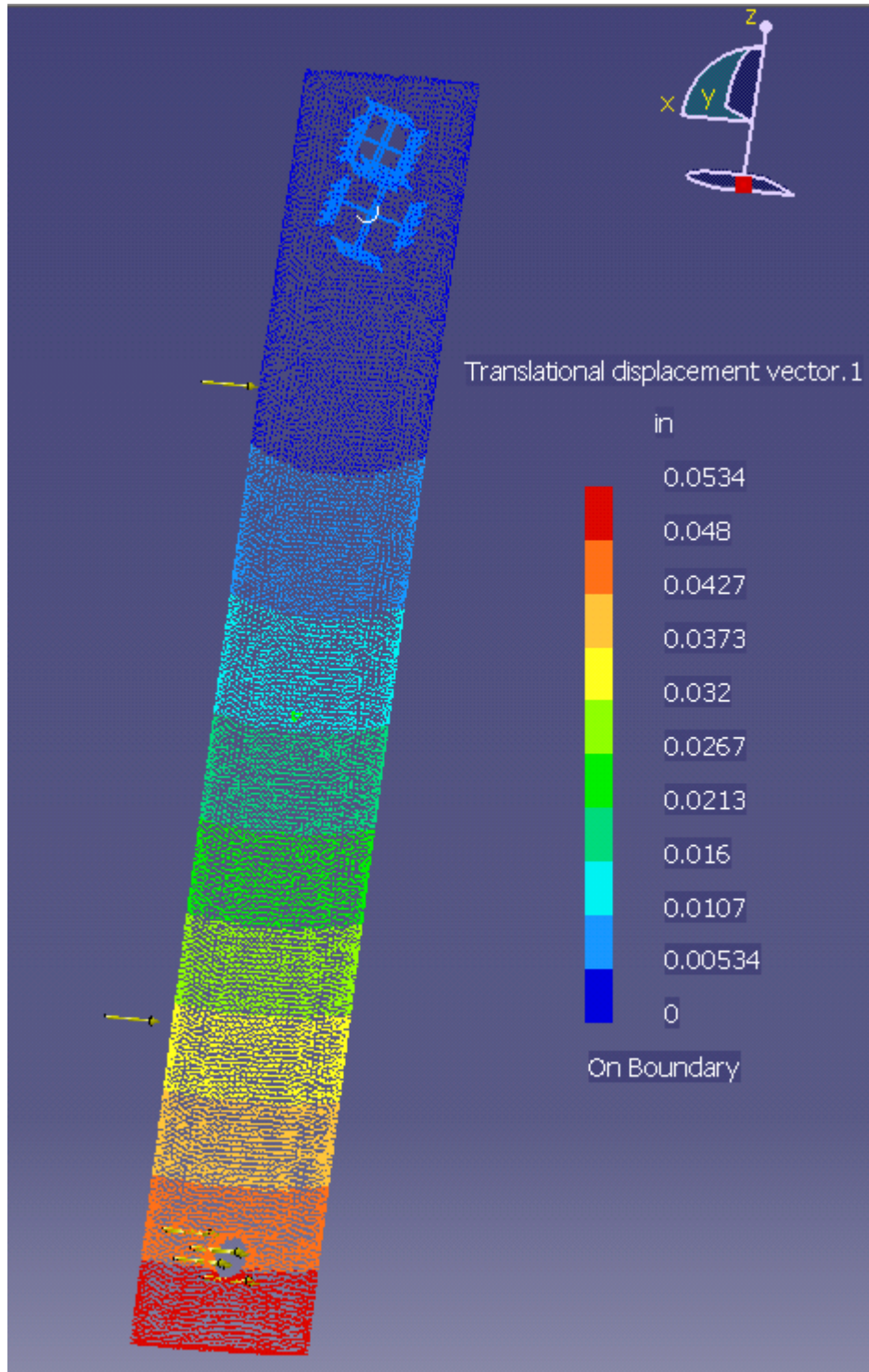


Figure 15: Displacements in the Strut

8. EXPERIMENTAL PROCEDURE

Flow Meter Correlation

The flow meter correlation was carried out by running the tunnel with an empty test section. The tunnel was run at various flow velocities ranging from 1 in/s to 6 in/s (recorded by the flow meter). For each reading of the flow meter, the corresponding velocity measured by the LDV was recorded and subsequently compared.

Flow Visualization

Pressurized dye was injected through the cylinder dye ports for varying flow velocities. The amount of dye injected was carefully monitored to match the flow velocity of the water in the tunnel and also to prevent the water from turning opaque too early in the experiment which would have prevented further LDV measurements from being made. Images were taken for each of the configurations and an analysis was done on the flow characteristics as a function of the Reynolds number. Flood lights were used to provide sufficient lighting for good images. A video camera was also used to record the flow development as it propagated downstream with the development of the Von Karman vortex street.

Frequency Distribution of Samples

A statistical analysis of the distribution of frequency of particles in the flow was carried out. In an empty tunnel with water flowing at 4 in/s, the oscilloscope was used to record a long data set over a 20 second time scale with the probe volume located in the midsection of the tunnel. The data recorded from the oscilloscope was then imported into a MATLAB script (given in the Appendix) from which, the peak frequency of the FFT was obtained at intervals of 10 ms which corresponds to the duration of a Doppler burst. Subsequently, the peak frequency from each of these truncated signals was plotted in the form of a histogram and the trend was compared to that of a Gaussian distribution for the probe placed in the free stream and in the wake.

Measurements in the Wake

LDV measurements were made in the wake of the cylinder. A 20 s dataset was captured

using the oscilloscope, this signal was then cut at intervals of 60 ms based on an analysis carried out to determine the deviation from the constant peak frequency over different averaged signal lengths as illustrated in Figure 16. For a signal length of 60 ms, the deviation from the constant value of the peak was $\sim 0.5\%$. The chosen signal length is also justified by the fact that for smaller signal lengths, the noise increases, while for longer lengths, the number of particles being averaged increases, leading to loss of information.

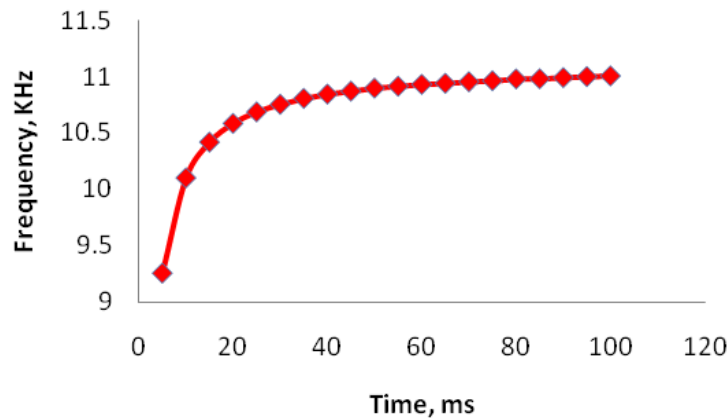


Figure 16: Variation in the peak frequency as a function of the chosen signal length in ms

The mean wake profile was obtained by moving the probe volume to the desired location in the wake; we then used the oscilloscope to record a data set, and repeated the process at different points across the width of the wake. The recorded data was then processed using MATLAB to determine the peak frequency from the FFT of the acquired signal within a given frequency range. This range was determined by analyzing the power spectrum on the entire 20s signal. We notice that there is a region of increased intensity, the width of which is dependent on the location of the probe volume and the corresponding particle frequency scatter. Figure 17 shows the FFT on the 20s signal in the free stream at 3in/s; notice that the region of increased intensity is narrow, going from 5.8 kHz to 7 kHz, whereas, in the wake, for example at $Re=2960$ (Figure 18), the region is wide, in this case from 3 kHz to 5.5 kHz.

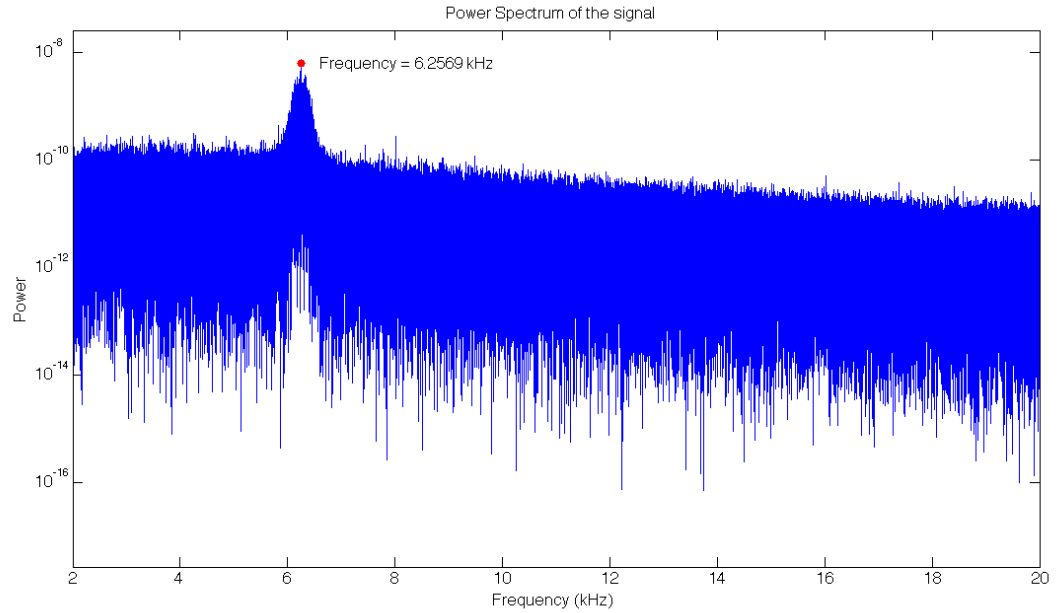


Figure 17: Power Spectrum of the 20s signal, in the free stream at 3in/s

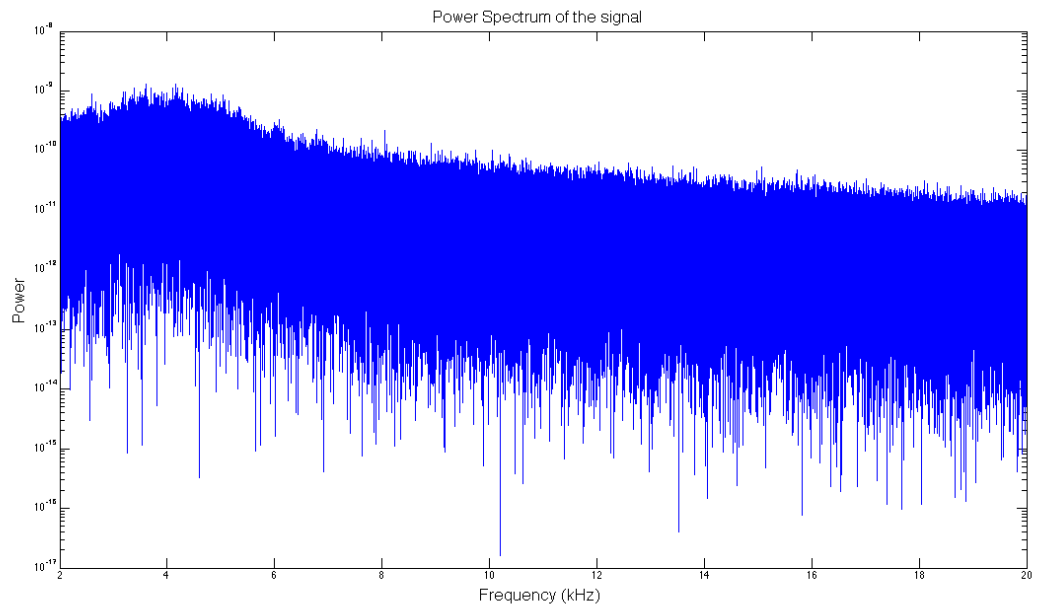


Figure 18: Power Spectrum of the 20s signal, in the wake at $z=0$ for $Re=2962$

We finally average all the frequencies that were computed every 60 ms. The average velocity at the probe location was then computed from the frequency shift and the mean wake profile was thus obtained corresponding to the desired downstream position and Reynolds number.

These velocity magnitudes could then be used to calculate the drag force (D) given by

$$D = h\rho \int_{-\infty}^{+\infty} u_l(U_\infty - u_l)dy$$

where ρ is the fluid density, h is the length of the cylinder, u_l is the velocity at the given location and U_∞ represents the free stream velocity

In order to perform the integration, we considered the function $f(y)$:

$$f(y) = u_l(U_\infty - u_l)$$

We then used the trapezoidal rule to obtain the required drag force acting on the cylinder. The trapezoidal rule for the numerical integration is given by

$$\int_a^b y dx \simeq \sum_{i=1}^{n-1} \frac{1}{2}(x_{i+1} - x_i)(y_{i+1} + y_i)$$

The coefficient of drag is related to the drag force in terms of the frontal area of the body (A) as

$$D = \frac{1}{2}\rho A U_\infty^2 C_d$$

The computed C_d was then compared for different Reynolds numbers.

Measurement of Fluctuations

The fluctuations were measured in the wake and in the free stream for different flow speeds. The procedure involved in capturing the data was similar to the one used to obtain the mean wake profile. After acquiring the long data set from the oscilloscope, the data was processed using MATLAB. The 20 second signal was cut into signals of 60 ms each to capture sufficient number of particles in the time interval. The peak of the FFT in the signal corresponding to each of the truncated signals was then plotted about the mean value to obtain the fluctuations over the length of the signal.

9. RESULTS AND DISCUSSION

a. Calibration

The tunnel was initially run without a model in the test section and subsequently a comparison was made between the flow meter readings and the velocities recorded by the LDV. Measurements were made for different flow speeds, ranging from 0.05 m/s to 0.18 m/s. Figure 19 represents the tabulated data.

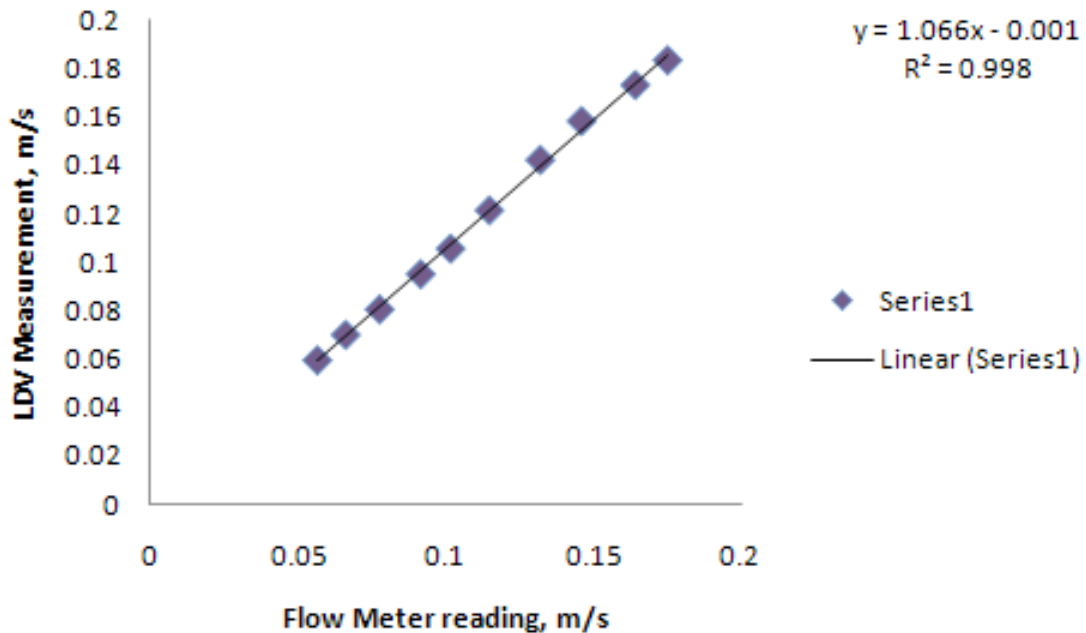


Figure 19: LDV calibration

A deviation of ~6.7% was noticed between the LDV and the flow meter readings. This deviation can be attributed to the inherent error involved in measuring the angle between the 2 intersecting laser beams. This may also be due to the flow meter being calibrated for a volume of water that was different from the volume at which the current analysis was done.

b. Flow Visualization

Characterizing the flow field based on the observations was one of the primary objectives of setting up the apparatus in the water tunnel. The dye traces were observed for varying Reynolds numbers. An estimate of the eddy formation length, L_f has been obtained through image

processing techniques. Image processing techniques have also been used to estimate the angle at which the free shear layer departs from the cylinder surface and has been defined with respect to the free stream direction. We have used the angle θ , as a means of observing a trend in the point of separation for varying Reynolds numbers. A schematic representation of the angle is shown in Figure 20. A higher Θ directly relates to early separation.

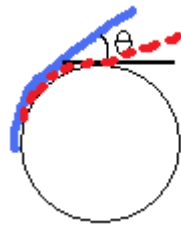


Figure 20: Schematic of the parameter used to determine the separation point

It is extremely important to match the dye injection velocity with that of the oncoming fluid velocity. A large deviation from the fluid velocity leads to incorrect flow representation by the dye trace. An illustration of the result of injecting dye with no flow is shown in Figure 21. The effect of buoyancy can be seen clearly in this illustration. The dye has a density which is greater than that of the water used in the tunnel. A more accurate representation of the flow may have been achieved if the density of the dye was reduced. This may have been possible with the addition of some alcohol in the mix. However, the trade off lies in capturing images with distinct dye traces and that of an accurate representation of the flow field. The dye trace in the figure can clearly be seen flowing over the top surface of the cylinder.

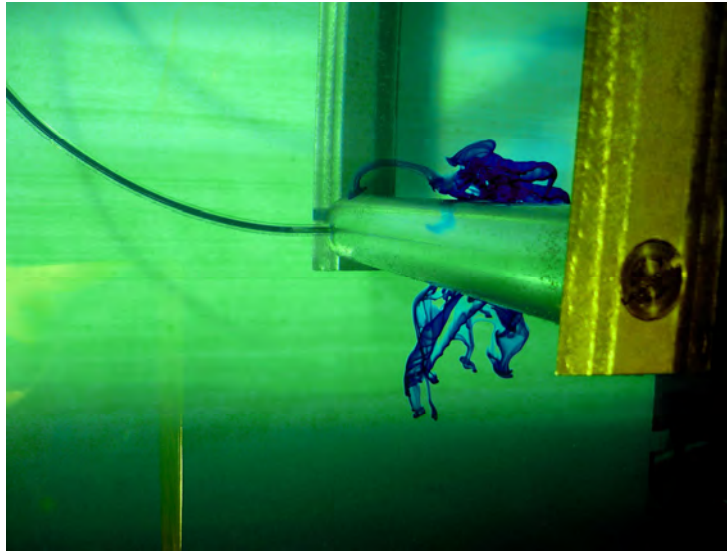


Figure 21: Visualization with no flow in the tunnel

An unsteady simulation of the problem was carried out to illustrate the development of the flow field. The results of the simulation are shown after 260 time steps. The simulation was done for a unit diameter with a flow speed of 0.3 m/s. Figure 22 shows the formation of the confluence point (C) in the near wake region of the cylinder with the velocity vectors colored by the magnitude. This point is characterized by the movement of the fluid in 4 different directions as indicated by the arrows marked in red, forming a free stagnation point. The dotted line in red indicates the presence of the free shear surface. Figure 23 illustrates the instantaneous velocity contours of the unsteady solution after the same number of time steps. The path taken by the fluid as it passes through the wake is indicated by the black solid lines marked with arrows, indicating the direction of flow. It clearly shows that the fluid from the free stream is entrained into the wake at the end of each eddy formation zone. The entrainment of the turbulent fluid from the confluent region renders the eddies turbulent.

Summary of the model:

Viscous, laminar, unsteady solution for flow over a circular cylinder

Fluid: water

Discretization Scheme: Pressure based, Second Order Upwind scheme

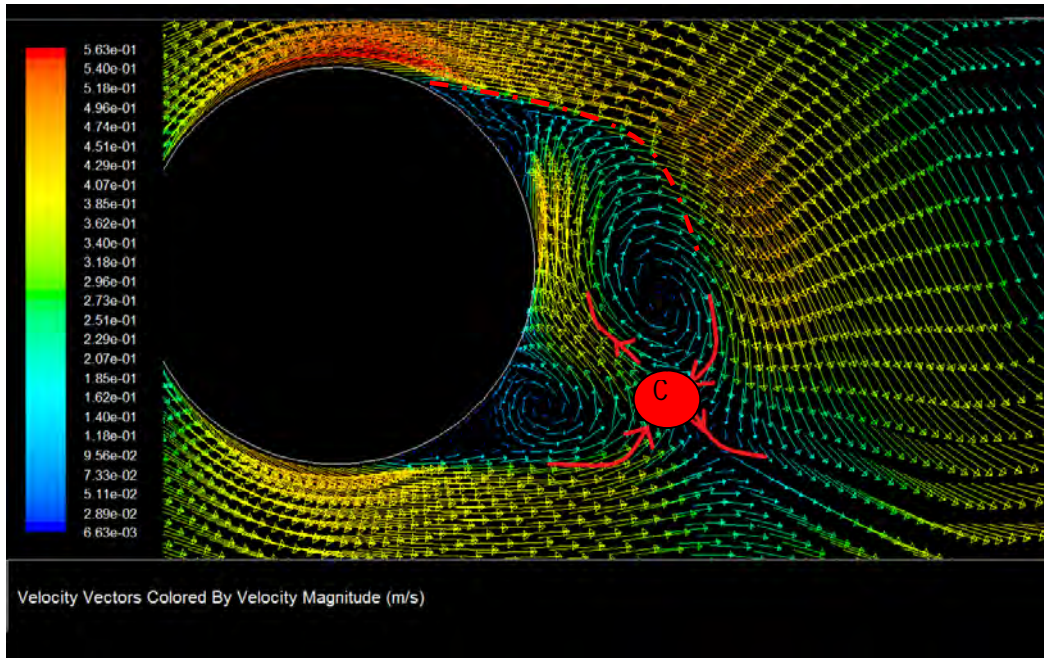


Figure 22: Instantaneous magnified image of the simulated flow domain indicating the presence of the confluence point in the wake after 260 time steps

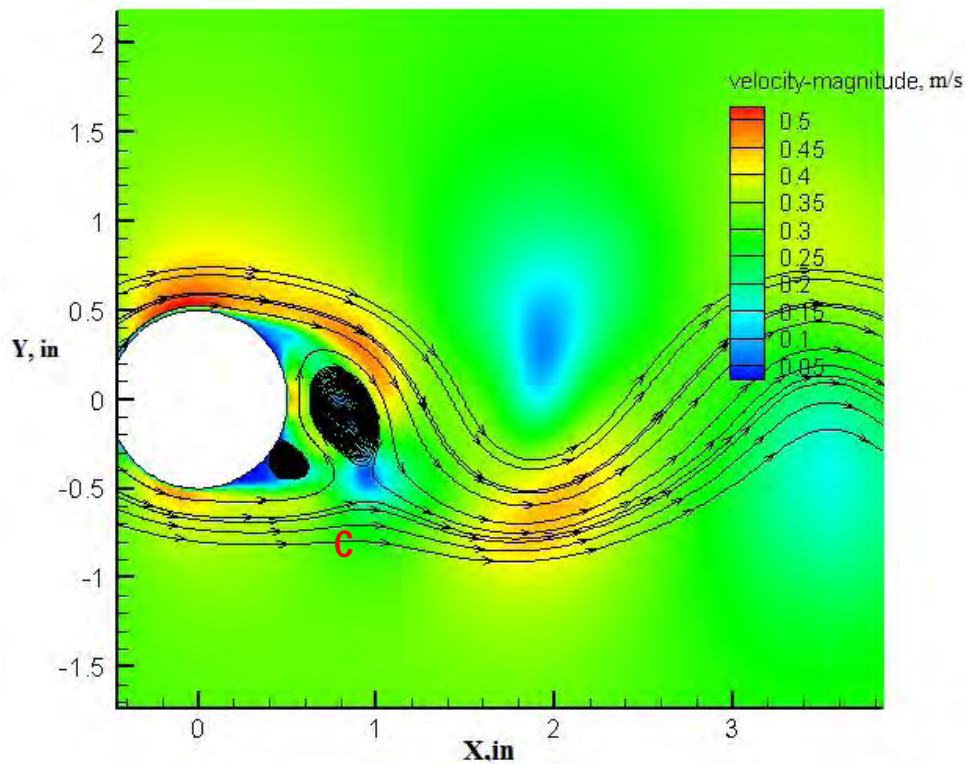


Figure 23: Instantaneous magnified image of the simulated flow domain indicating the flow path superimposed on the velocity contours of the unsteady flow solution

Figure 24 represents the flow field for a Reynolds number of ~ 900 . Flow in this range of Reynolds numbers is characterized by the onset of transition in the shear layers and the development of turbulence in the wake further downstream. The near wake is surrounded by a laminar shear layer. The shear layer becomes turbulent before rolling up into turbulent eddies. Transition waves referred to as Gerard-Bloor waves develop along the shear surface. The transition waves are seen as undulations on the shear surface, originating from the separation point. Thus they originate in the boundary layer itself and are not caused by the eddy shedding pattern. This is followed by the formation of transition eddies which precede the transition to turbulence. The eddies thus become irregular further downstream once the turbulence sets in. The vortex shedding frequency is estimated to be at ~ 0.69 Hz (based on a Strouhal number of 0.2). In this flow regime, the reduction in the eddy formation length with increasing Reynolds number is accompanied with an increase in thickness of the shear surface, thus maintaining the Strouhal number at ~ 0.2 . The development of a distinct Von Karman Vortex street was seen and is illustrated in the figure. The eddy formation length, L_f for this flow configuration was found to be at $\sim 2.8D-2.9D$ from the cylinder. However, L_f reduces with increase in the Reynolds number, bringing the eddies close to the cylinder and continuously shifting the transition towards the separation point. Θ is estimated to be 4.3° for $Re=900$. The expected confluence point is marked in Figure 25 for the same flow configuration and is at ~ 1 diameter away from the cylinder. The dye trace indicating the flow path taken up by the fluid in the wake seems similar to that simulated and is marked by the 2 solid lines in red. The dotted line indicates the extent of the free shear surface. The fluid from the free stream is entrained into the wake at the end of the eddy formation zone. The confluence point marks the position of the free stagnation point in the wake.

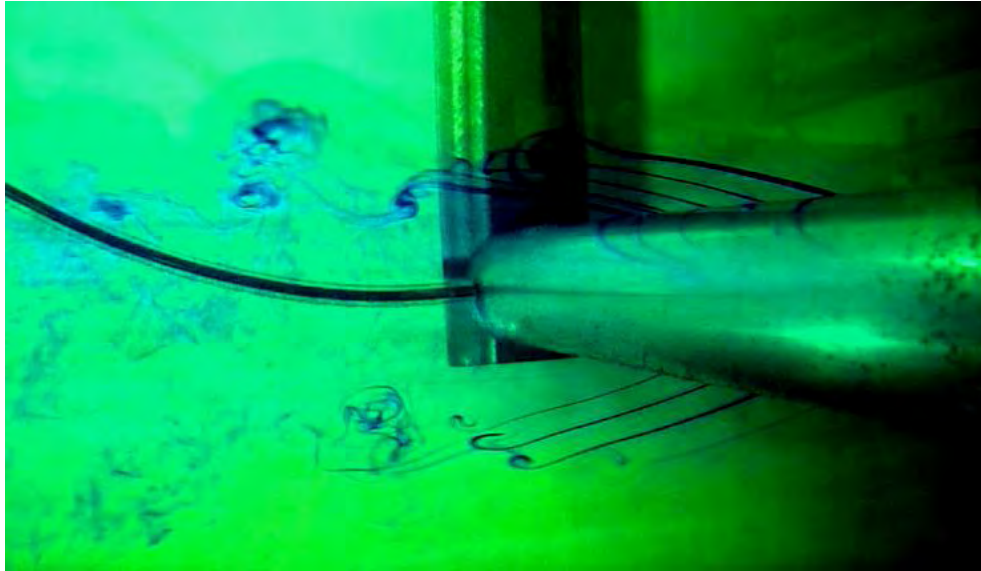


Figure 24: Free shear layer and delayed eddy curl up in the shear layer at Re of 900

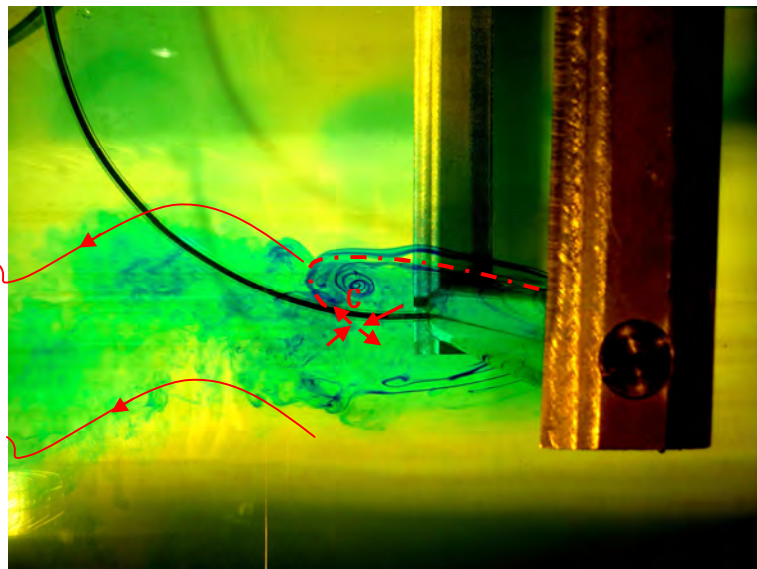


Figure 25: Formation of the confluence point and the free shear layer with the arrows indicating the entrainment of the free stream between the shed eddies at Re of 900

Initially, the eddy shedding is initiated as a trail instability and then rolls up along the shear layers. The eddies grow as they move downstream. As the Reynolds number is increased, the eddies develop in almost fixed locations which then diffuse and decay along their movement downstream. The shedding pattern comprises of the following pattern; it comprises of the roll up

of the shear layer which then ceases when the eddy gets disconnected from the shear surface. Once the eddy grows large enough to draw the shear surface from the opposite end, it gets cut off and is finally shed.

Figures 26–27 represent the flow field for Reynolds numbers 5400 and 9000 respectively. Comparing the flow fields with those obtained at lower Reynolds numbers as represented by Figure 24, it is clear that L_f is much smaller when the Reynolds number is higher. In order to estimate this trend, we performed an analysis of the flow field using image processing techniques. A camera was mounted at a fixed position and images were captured for different Reynolds numbers from the same position. A scale was used to relate the number of pixels to the linear dimension in the tunnel. The Table 3 summarizes the observed trend in L_f as a function of the Reynolds number. The obtained trend matches the predictions of (Bloor S.M, 1964) within 7%. The magnitude of the angle θ is also shown in Table 3. The observed trend indicates that the separation point moves towards the front stagnation point as the Reynolds number is increased, thus increasing the value of θ with increasing Reynolds number. The values of the angle θ obtained matches well with flow visualization studies performed previously. An analysis of the visualization done by (Werle and Gallon, 1972) showed that the angle θ for a Reynolds number of 2000 was $\sim 8^\circ$. Similarly, Thomas Corke and Hassan Nagib imaged the flow at a Reynolds number of 10,000 and an analysis predicted the angle to be $\sim 25^\circ$.

In order to visually inspect the vortex shedding frequency, we captured a video of the flow over the cylinder. The vortex shedding frequency was found to be ~ 0.8 Hz for a velocity of 5.1 in/s from the video captured. This compares well with the expected frequency of 0.69 Hz for a Strouhal number of 0.2.

Reynolds Number	L_f	Θ, degrees
900	2.8 D-2.9 D	4.3
1800	2.4 D-2.5 D	5.2
2700	2 D-2.2 D	7.2
3600	2 D- 2.1 D	7.5
4500	1.5 D-1.6 D	12.9

5400	1.4 D-1.5 D	15.4
6300	1.39 D-1.5 D	14.8
7200	1.36 D	23.6

Table 3: Summary of Predicted trend in Separation and Eddy Formation distance in the Free Shear based on Image Processing

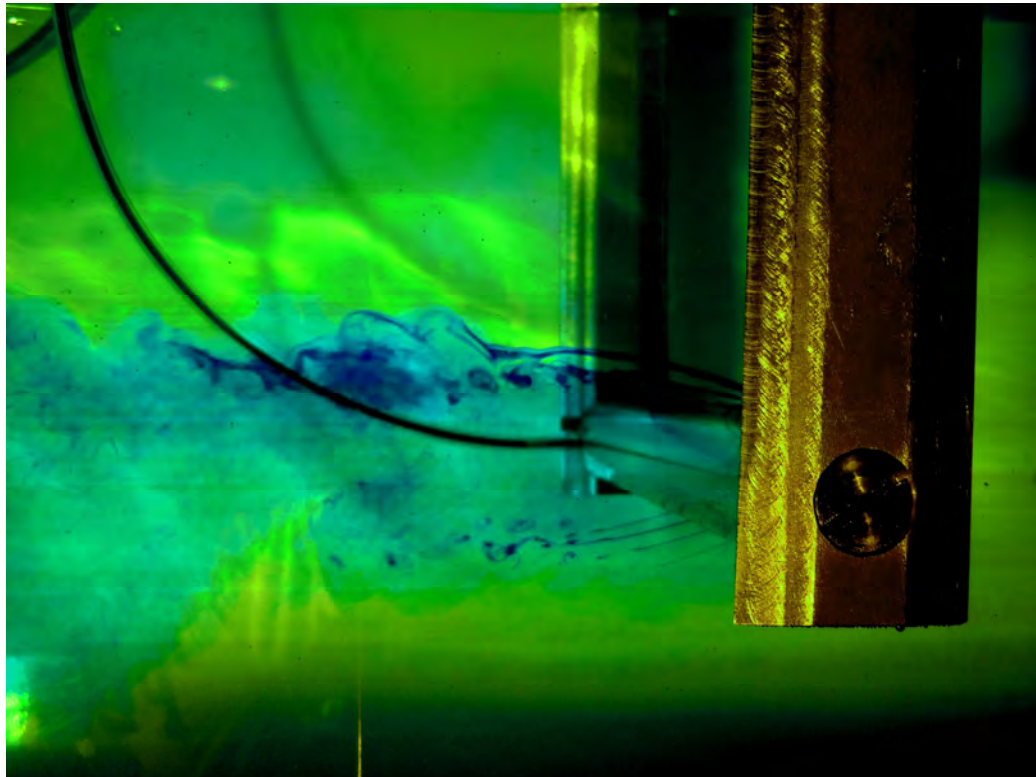


Figure 26: Flow at $Re=5400$, the eddy formation distance is much shorter when compared to the flow at $Re=900$

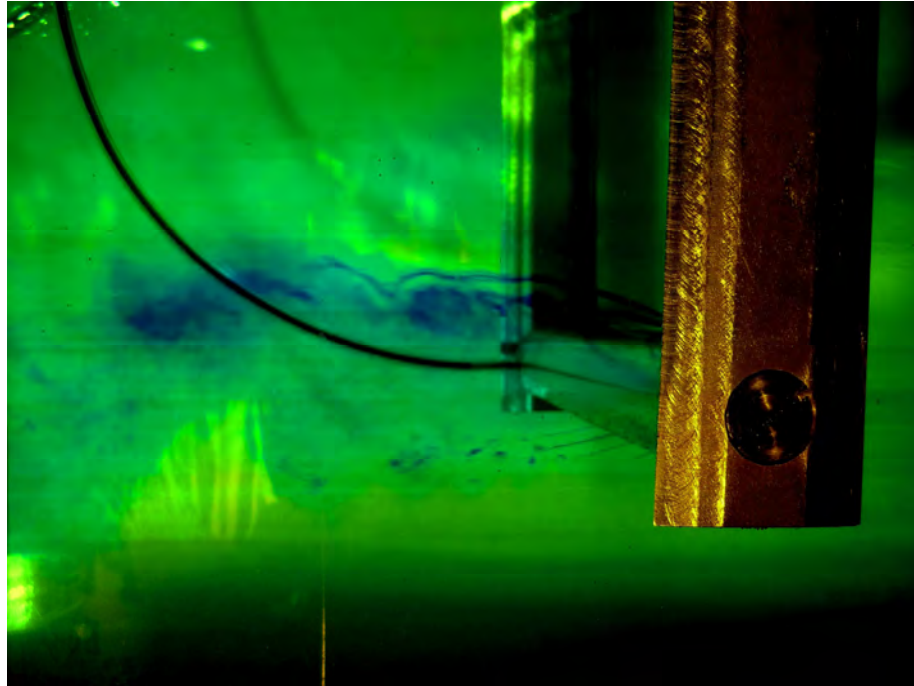


Figure 27: Flow at $Re=9000$, showing a large separation angle, indicating early separation along with turbulence in the wake

c. Statistical Analysis

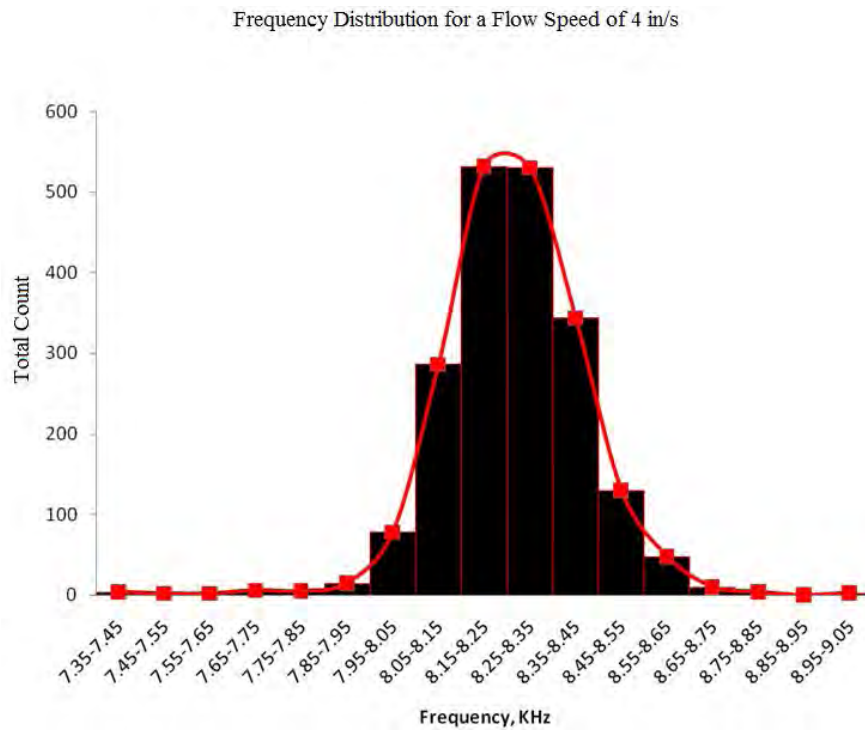


Figure 28: Frequency distribution of each truncated signal at a flow speed of 4 in/s

Due to the manner in which measurements using the LDV are taken, they are characterized by errors due to variations in the flow properties between individual particles. In order to estimate the error involved in assuming that measurements of a single particle represent the flow characteristics of the entire flow field, a statistical analysis was carried out. For a flow speed of 4 in/s, a 20 second record was captured using the oscilloscope in the mid-section of the empty tunnel. The acquired record was truncated into signals of 10ms length (based on the doppler burst frequency). The peak frequency from the FFT of each truncated signal corresponding to each particle passing through the probe volume was plotted. The associated frequency of the truncated signals are grouped and represented in Figure 28. The clustering of the sample frequencies around the mean value leads us into believing that the frequency distribution follows a bell shaped curve and can be represented by a Gaussian distribution. This forms an extremely important part of the analysis since a wide distribution would reduce the accuracy of the measurements that are taken using the LDV technique, making it hard to obtain a distinct peak in the power spectrum.

An analysis of the data captured in the free stream and in the wake at 5 D from the cylinder was carried out. The analysis of the data from the free stream is shown in Figures 28-29. Figure 29 has been superimposed with the Gaussian distribution and shows the extent of conformance between the observed and predicted data. The frequency distribution has a mean of 8.27 kHz with a standard deviation of 0.154. It was found that only 30.41% of the samples had a frequency greater than the mean by 1%. 99.25% of them lie within 5% on either side of the mean and 89.16% of them lie within 3% on either side of the mean. Comparing this with the analysis carried out at 5 D in the wake, there is a large deviation from the Gaussian distribution that we see in the free stream. The mean of the frequency distribution was found to be at 4.27 kHz with a standard deviation of 1.67. 49.02% of the samples had a frequency on the lower side of the mean by more than 1% while 48.9% of them had frequencies more than 1% above the mean. Only 10% of them lie within 5% on either side of the mean and 6.1% of them lie within 3% on either side of the mean. Thus the particle frequencies have a much larger scatter and lead to a broad peak in the power spectrum for measurements in the wake. As a consequence of this, obtaining the peak of the frequency in the wake of the cylinder becomes hard as compared to obtaining the

peak in the free stream. Figures 30 - 31 show the sample frequency distribution at a distance of 5 D and 7.5 D in the wake respectively. It clearly indicates that there is an increase in the number of particles that possess lower frequencies in the wake.

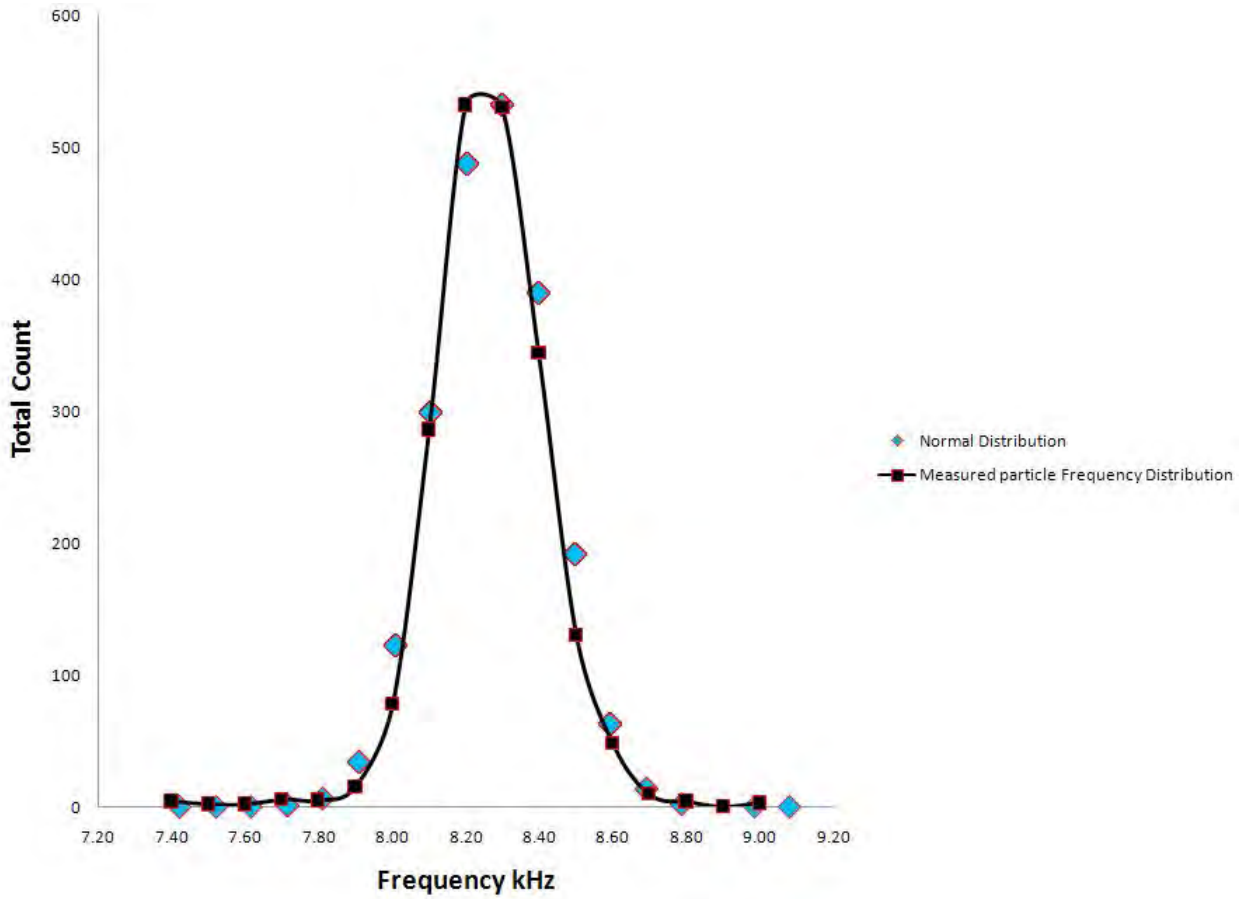


Figure 29: Comparison of measured frequency distribution with the Gaussian distribution

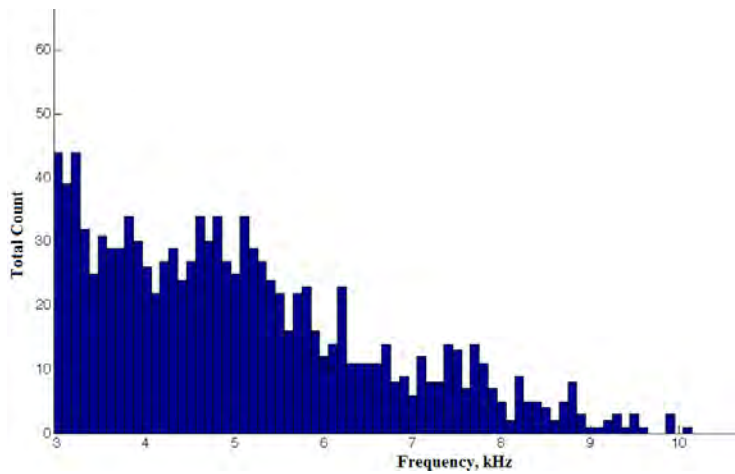


Figure 30: Sample frequency distribution in the wake at a distance of 5D

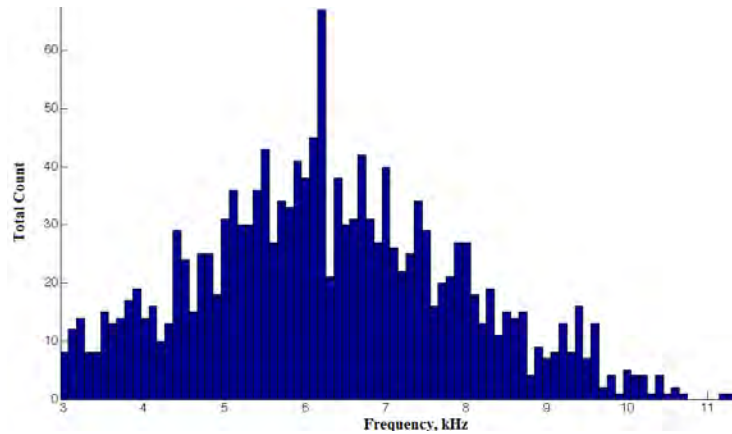


Figure 31: Sample frequency distribution in the wake at a distance of $7.5D$

d. Wake Profile

As the fluid passes over the cylinder, the pressure reaches a maximum value at the stagnation point and gradually decreases along the front half of the cylinder. The pressure being favorable in this half of the cylinder, the flow remains attached. However, the pressure starts to increase in the rear half of the cylinder and the fluid begins to experience an adverse pressure gradient. Consequently, the flow separates from the surface, creating a highly turbulent region behind the cylinder, forming the wake. The pressure inside the wake remains low as the flow separates and a net pressure force is produced which comprises the pressure drag. The drag can be represented in a non-dimensional form given by the coefficient of drag, C_d . The velocity deficit experienced in the wake of the cylinder for different Reynolds numbers is shown in the Figures 32-33. The deficit is found to be greater for larger Reynolds numbers than it is for smaller Reynolds numbers. The wake profile was measured for three different Reynolds numbers and a comparison was done between the use of a hot wire anemometer in the wind tunnel and the LDV technique in the water tunnel for measuring the mean wake profile for the same Reynolds numbers. Figure 32 represents the wake profile as measured in the water tunnel using the LDV technique while Figure 33 represents the wake profile as captured by measurements using the hot wire in the wind tunnel.

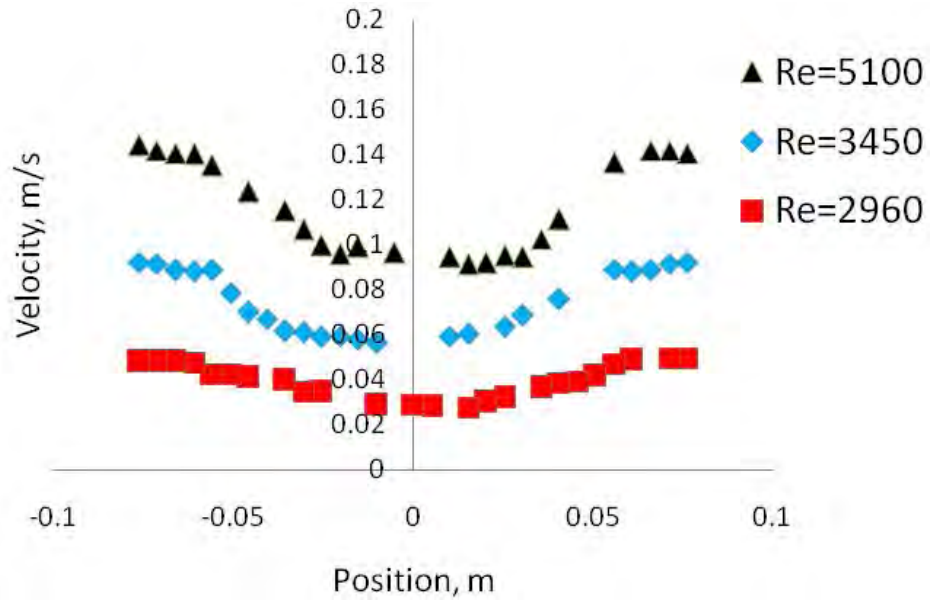


Figure 32: Mean wake profile at 7.5D behind the cylinder measured using the LDV

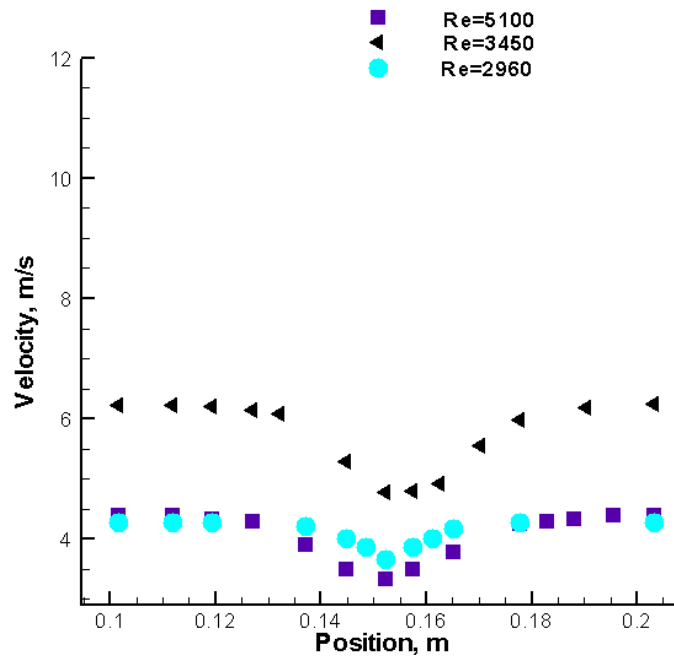


Figure 33: Mean wake profile at 7.5D measured using the hot wire

Reynolds Number	Experimental Correlations, Cd	LDV measurements, Cd	% Deviation	Hot Wire Measurements, Cd	% Deviation
5100	1.03	1.09	5.8	1.1	6.8
3450	1.04	1.23	18	1.12	7.6
2960	1.08	1.24	14.8	1.2	11.5

Table 4: Comparison of the measured Coefficient of Drag using the LDV and the Hot Wire techniques in the Water Tunnel and Wind Tunnel Respectively

It was found that the LDV technique performs well for higher flow speeds and as illustrated in the case with a Reynolds number of 5100, the measured Cd in the water tunnel was found to deviate from the predictions of experimental correlations by 5.8% while the measurements made in the wind tunnel using the hot wire probe deviated by 6.8%. However, comparing the measured Cd using the two techniques at lower Reynolds numbers, the percentage deviation of the measurements in the water tunnel from the predictions of experimental correlations was higher than in the wind tunnel using the hot wire. This has been illustrated using the flow at a Reynolds number of 2960 where the percentage deviation using the LDV technique was found to be 14.8% while that using the hot wire probe was found to be 11.5%. This observation could be attributed to the following reason; it was shown in the statistical analysis that using the LDV to measure the peak frequency of the FFT was an arduous task, given the frequency distribution in the wake of the cylinder. This was found to be prominent when the velocity deficit was small (when the Reynolds number was small). A summary of the computed Cd and the experimental correlations are shown in Table 4.

e. Fluctuations

i. General Approach

As with the analysis described earlier, a 20 seconds signal was captured and imported into MATLAB for processing. Truncated signals of 60 ms each were output and an analysis of the obtained power spectrum helped finding the average particle frequency corresponding to each of the truncated signals. This gave us a vector, representing the evolution of the peak

frequency every 60 ms. Figure 34 is a representation of the fluctuations in the free stream for a flow speed of 3 in/s.

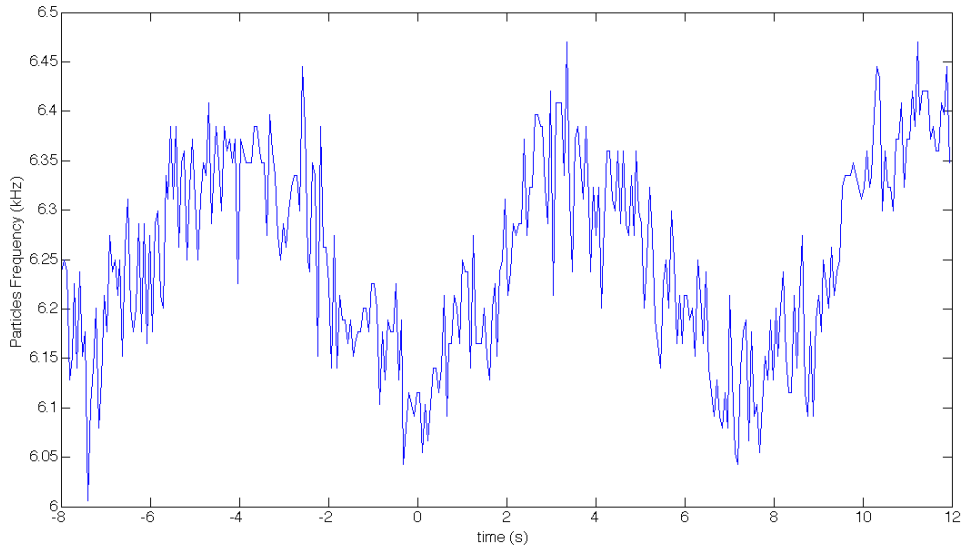


Figure 34: Fluctuations in the free stream for a flow speed of 3 in/s (Raw Signal)

It was observed that a high frequency noise overlapped the low frequency fluctuations of ~ 7.5 s period. In order to eliminate this, an average of every 15 consecutive points was taken (Figure 35). This number is arbitrary and depends on the signal; it requires various attempts to eliminate the noise without losing the trend of the original signal. Consequently a plot of the percentage fluctuations centered on the x-axis about the mean was obtained. It represents the deviation of the frequency as a percentage about the mean.

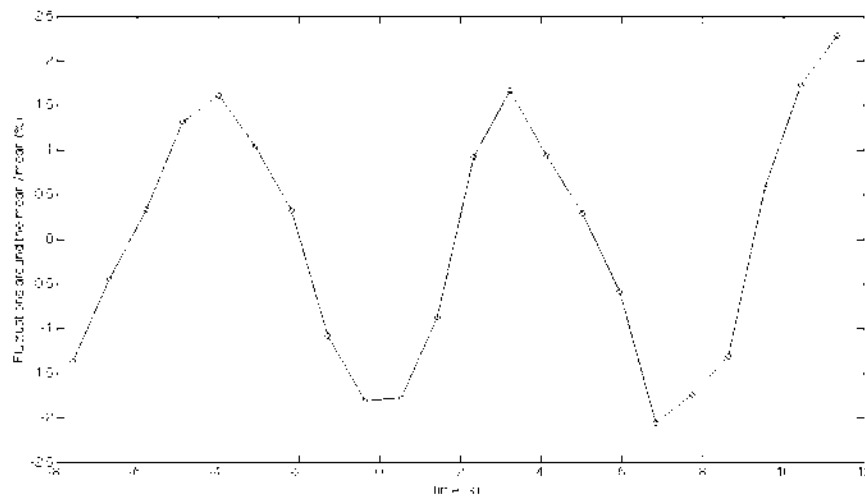


Figure 35: Fluctuations in the free stream for a flow speed of 3 in/s (Smooth Signal)

Notice that the period of the signal still remains at ~ 7.5 s while the noise has been eliminated.

ii. Fluctuations in the free stream at different Flow Speeds

In order to study the fluctuations introduced in the flow as the flow rate was varied, we carried out an analysis in an empty test section. The procedure adopted to capture the signal and process the data was similar to those described earlier. The resultant plot giving the percentage deviation from the mean for various flow speeds is shown in Figure 36.

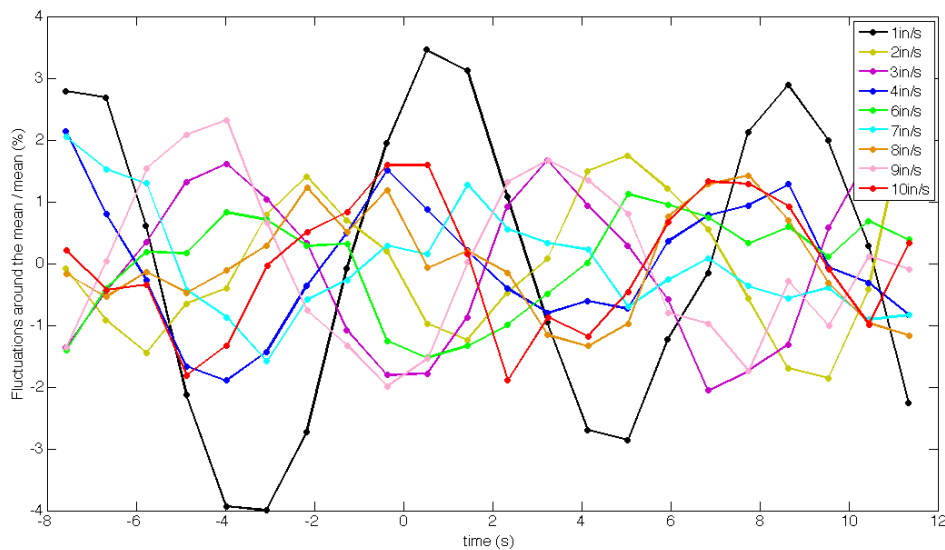


Figure 36: Fluctuations in the free stream for different flow speeds

It was noticed that the fluctuations in the flow varied between 1.5-2.2% between speeds of ~2 in/s to 10 in/s. However, when the flow speed was dropped to 1 in/s, the fluctuations increased to 4% as shown in the Figure 36. This trend explains the inability to control the flow rate of water in the tunnel between 0-1 in/s.

We thus have a maximum of 4% deviation when the tunnel is run at 1 in/s; then the deviation drops to ~2% for a flow speed between 2-4 in/s. Beyond that, it decreases to 1.5% at 8 in/s and finally, increases to ~2.2% for flow speeds ranging between 9 in/s and 10 in/s. The increase in the fluctuations at velocities beyond 9 in/s could be attributed to disturbances that may have been present due to the struts or the surface effects may have played a dominant role for such flow speeds.

In order to visualize this trend better, we plotted the maximum deviation about the mean as a function of the flow speed (Figure 37).

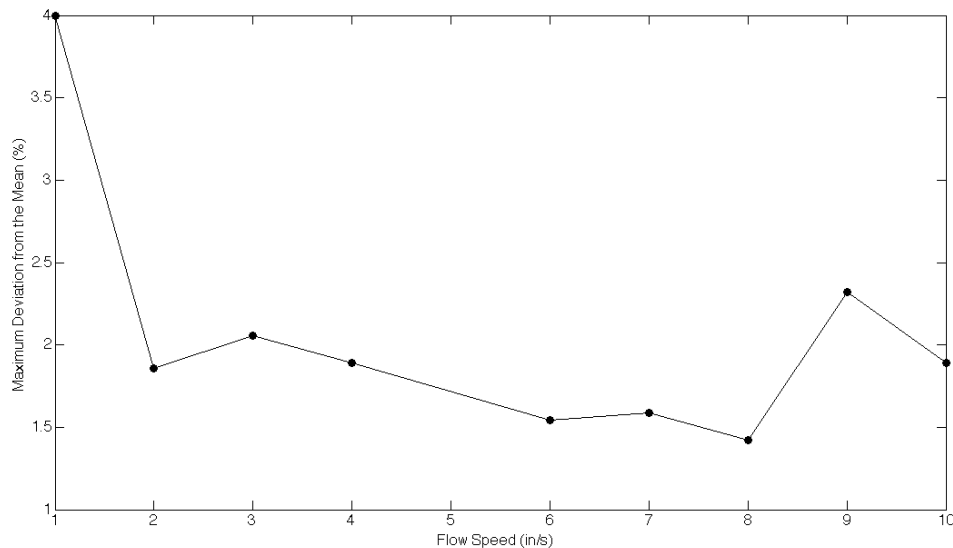


Figure 37: Fluctuations in the free Stream as a function of the flow speed

iii. Fluctuations in the wake

For a Strouhal number of 0.2, the expected vortex shedding frequency is ~0.69Hz which corresponds to a period of 1.47s. Therefore, cutting the signal every 60 ms, would give us ~24 points per period. Figure 38 shows the fluctuations in the wake of the cylinder at $x=7.5 D$, $y=0$, $z=0$ and $Re=5100$.

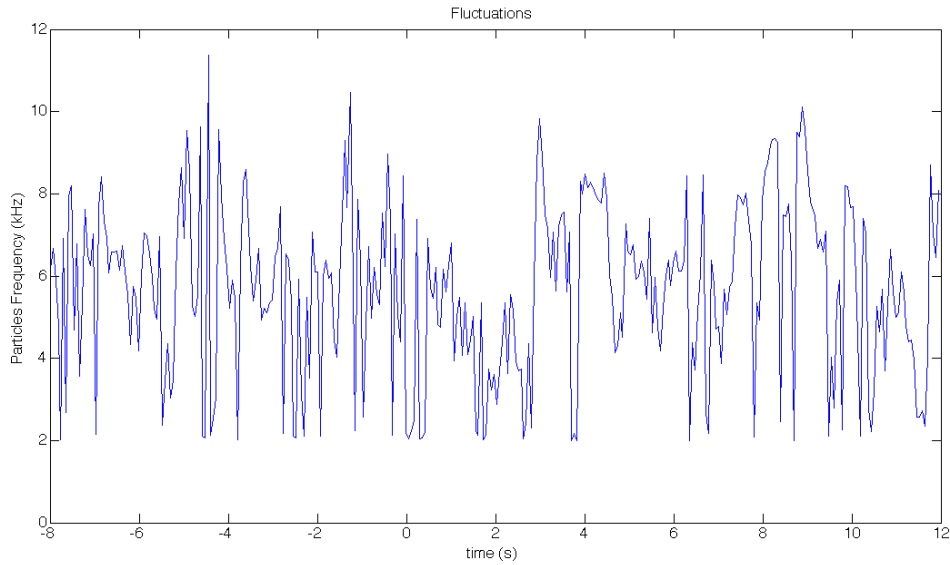


Figure 38: Fluctuations downstream at $x=7.5D$, $y=0$, $z=0$ and $Re=5100$

The fluctuations observed did not follow any particular trend that could be predicted from theory. On applying the same method as in the free stream study (averaging the signal for a large number of points to smooth it out), we were not able to obtain sufficient number of points over one period. Averaging every 2 points, giving us 12 points per period does not eliminate the noise completely as shown in Figure 39.

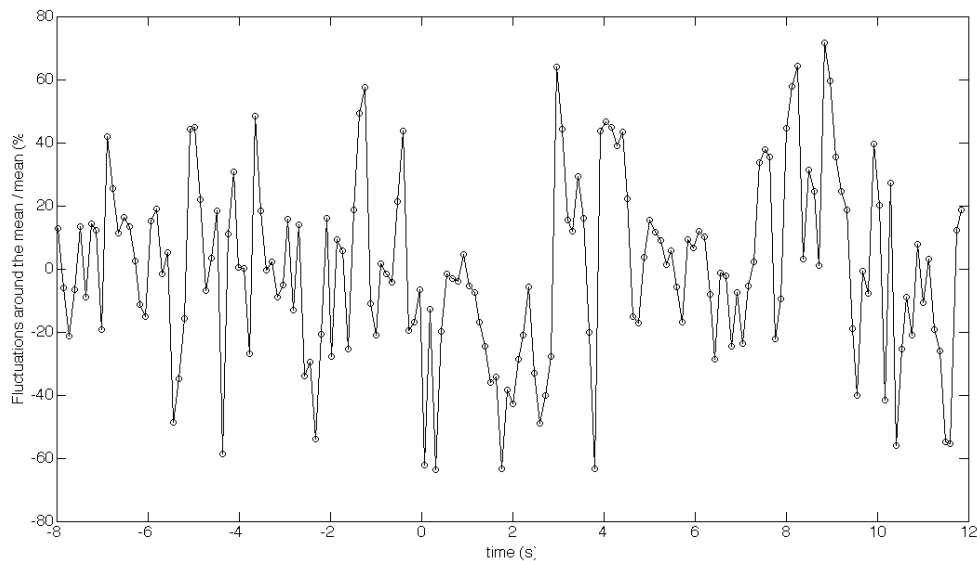


Figure 39: Fluctuations in the wake at $x=7.5D$, $y=0$, $z=0$ and $Re=5100$, averaged every 2 points

The expected signal frequency of ~ 0.69 Hz could not be obtained in the wake. Figure 40 shows the power spectrum of one truncated signal. Notice that there is no distinct peak in the spectrum; the peak is at ~ 0.20 Hz but we still have other frequency spikes almost as high as the identified peak. Thus it was found that characterizing the fluctuations in the wake using the LDV was difficult and the trend was found to be worse when the measurements were made closer to the cylinder. This has also been verified by the statistical analysis.

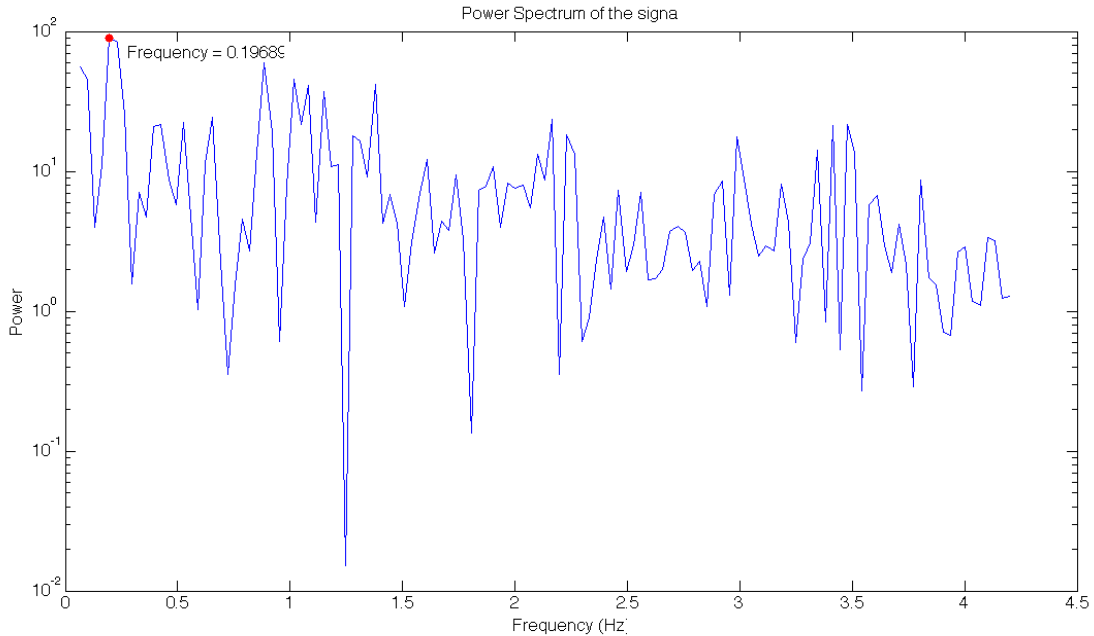


Figure 40: Power spectrum of the signal shown on Figure 39

10. CONCLUSIONS

An experimental study involving the use of a water tunnel to analyze the flow around a circular cylinder using dye flow visualization technique has been discussed. LDV techniques have been used to quantify the flow field characteristics. Flow visualization aided the observation of vortex formation, boundary layer separation and transition to turbulent flows in the wake. The observed dye traces were compared to visualization techniques used earlier and with the results of an unsteady simulation of flow around a circular cylinder. The observed angle at which the free shear layer departs the cylinder surface and the length to eddy formation in the wake has been quantified through image processing techniques. It was found that L_f reduced

from 2.8 times the diameter for a Reynolds number of 900 to ~1.3 times the diameter when the Reynolds number was increased to 7200. Similarly, the angle, θ increased from 4° to 23° for the same range of Reynolds numbers. A statistical analysis of the flow pattern in the free stream and in the wake has been done. It was observed that the particles frequency followed a near Gaussian distribution in the free stream with 89.16% of them lying within 3% on either side of the mean of the distribution. On the other hand, the frequency distribution in the wake of the cylinder was found to have a large scatter with only 6.1% of them lying within 3% on either side of the mean. Measurements were also made to study the wake profile for different Reynolds numbers and a comparison was made with experimental correlations. A comparison has been made between the use of hot wire anemometry techniques and LDV techniques for measuring the mean wake profile in the wind tunnel and the water tunnel respectively. It was observed that the measurements made using the LDV technique matched the predicted coefficient of drag for higher Reynolds numbers better than that for lower Reynolds numbers. The deviation for a Reynolds number of 5100 was ~6%, while it increased to 15% for Reynolds numbers of ~ 2960. This was attributed to the increase in particle frequency scatter. The current work also involves the measurement of the fluctuations in the free stream as a function of the flow speed. It was found that the fluctuations in the free stream increased at flow speeds approaching 1 in/s where the fluctuations were found to be at 4%, while that at flow speeds of 10 in/s were at 2% of the mean. The fluctuations measured in the wake of the cylinder did not follow any expected trend and was worse when the measurements were made closer to the cylinder in the wake. Thus it was not possible to make any inference from the fluctuations measured in the wake close to the cylinder.

11. ACKNOWLEDGEMENTS

The authors gratefully acknowledge the guidance provided by Prof Steven Schneider and Ted Londner and would like to thank them for the extremely useful discussions through the course of the project. The authors would also like to thank Madeline E Chadwell and Jerry Hahn for the fabrication of the setup and the financial support provided from Purdue University through the course differential fee.

12. REFERENCES

- Achenbach, E., Distribution of local pressure and skin friction around a circular cylinder in cross-flow up to $Re = 5 \times 10^6$, *J. Fluid Mech.* 34, 625-639, 1968
- Achenbach E. 1971. Influence of surface roughness on the cross-flow around a circular cylinder. *J. Fluid Mech.* 46:321–35
- Achenbach, E., The effect of surface roughness on the heat transfer from a circular cylinder to the , *Int. J. Heat Mass Transfer* 20, pp. 359–369, 1977
- Beckner C. and Curry R. E., *Water Tunnel Flow Visualization Using a Laser*, NASA Technical Memorandum 86743, 1985
- Bloor S.M., The transition to turbulence in the wake of a circular cylinder., *Journal Fluid Mechanics.*, 19, pp. 290-309, 1964
- Campbell D.R, *Flow Visualization Using a Selectively Sensitive Fluorescent Dye*, Aerospace Res. Lab. Rep. ARL 73-005, 1973
- Clayton B.R and Massey B.S, *Flow Visualization in Water: A review of Techniques*, *J. Sci. Instrum.*, 44, pp. 2-11, 1967
- Cummins H.Z, N Knable and Yeh Y, *Observation of Diffusion Broadening of Rayleigh Scattering Light*, *Phys. Rev. Lett.*, 12, pp. 150-153, 1964
- Eidetics International Inc., *Preproduction Flow Visualization Water Tunnel*, 2004
- Erickson G.E, *Vortex Flow Correlation*, Air Force Wright Aeronautical Lab. Rep, AFWAL TR 80-3143, 1981
- Farell, C., *Proc. A.S.C.E.: J. Engng Mech.* 107 (EM3), 565, 1981
- Foreman J.W., Jr., Lewis R.D, thornton J.R and Watson H.J, *Laser Doppler Velocimeter for Measurements of Localized Flow Velocities in liquids*, *IEEE Proc.*, 54, pp. 424-425, 1966
- Foerster, S., *Determination of the geometrical position of vortices in flow fields visualized by laser light sheet*, *Flow visualization V; Proc. of the 5th International Symp.*, Prague, Czechoslovakia, Aug. 21-25, 1989
- Gerrard J.H, *The Wakes of Cylindrical Bluff Bodies at Low Reynolds Numbers*, *Phil. Trans. R. Soc. London Ser. A*, 288, p. 351, 1978

- Goldstein R.J and Kreid D.K, Measurement of Laminar Flow Development in a Square Duct using a laser Doppler Flow meter, J. Appl. Mech., 34, pp. 813-817, 1967
- Goldstein R.J and Hagen W.F, Turbulent Flow Measurements utilizing the Doppler Shift of Scattered Laser Radiation, Phys. Fluids, 10, pp. 1349-1352, 1967
- Guven, O., Farrell, C, Patel, V. C, "Surface Roughness Effects on the Mean Flow. Past Circular Cylinders," J. Fluid Mech, Vol. 98, pp. 673-701, 1980
- Guven, O, Patel, V. C and Farrell, C, Trans. A.S.M.E. I : J . Fluids Engng 99, 470, 1977
- Hama F.R, Streaklines in a Perturbed Shear Flow, Phys. Fluids, vol 5, no 6, 1962
- Hama F.R, Three Dimensional Vortex Pattern Behind a Circular Cylinder, J. Aeronaut. Sci., 24, p 156, 1957
- Hoffmann, A.; Zimmermann, F.; Scharr, H.; Krömker, S.; Schulz, C., Instantaneous three-dimensional visualization of concentration distributions in turbulent flows with crossed-plane laser-induced fluorescence imaging, Applied Physics B, Volume 80, Issue 1, pp.125-131, 2005
- James R.N, Application of a laser Doppler Technique to the measurement of particle Velocity of Gas particle Two-Phase Flow, PhD. Thesis, Stanford University, Stanford, 1966
- Jones. G.W Cincotta, J. J. & Walker R, W. NASA Tech. Rep. R-300, 1969
- Merykirch W., Flow Visualization, Academic, New York, 1974
- Milton Van Dyke, "An Album of Fluid Motion", Parabolic Press, 1982
- Kreid D.K., Measurements of the Developing Laminar Flow in a Square Duct: An Application of the laser-Doppler Flow meter, M.S thesis, University of Minnesota, Minneapolis, 1966
- Roshko, Anatol: Experiments on the Flow Past a Circular. Cylinder at. Very High Reynolds Numbers. J. FluidMech, Vol. 10, pt. 3., May. 1961
- Schlichting, H. Boundary-Layer Theory, 6th Ed., translation by Kestin J. Chs. 14 and 20 (1979) McGraw-Hill, New York.
- Shen, Gongxin, Laser spatial flow visualization and its application, Acta Aerodynamica Sinica (ISSN 0258-1825), vol. 10, no. 3, p. 283-292, 1992

- Smits, A.J and Lim T.T, Flow Visualization: Techniques and Examples, Imp. Coll. Press, London, pp 43-47, 2000
- Son J.S, Experimental and Computational studies of flow around a circular cylinder, Ph.D Thesis, Chemical Engineering Department, University of Illinois, Urbana, 1974
- Szechenyi, Supercritical Reynolds number simulation for ... flow over circular cylinders, J. Fluid Mech. 70 (3) pp. 529–542, 1975
- Tani, I. In Preprints of IUTAM Symp. on Concentrated Vortex Motions in Fluids 1964
- Tani, I., J.Japan Soc. Aero. Sci. 15, 426, 1967
- Toaktaty GA, A History and Philosophy of Fluid Mechanics, Foulis, Oxfordshire, U.K., 1971
- Węclaś, M.; Melling, A.; Durst, F, Combined application of surface flow visualization and laser-Doppler anemometry to engine intake flows, Experiments in Fluids, Volume 15, Issue 4-5, pp. 323-331, 1993
- Werle H. Hydrodynamic Flow Visualization, Annu. Rev. Fluid Mech., 5, pp. 361-382, 1973
- Werle, H., and Gallon, M., “Controle d' Élements par Jet Transver- sal,” ONERA, Extrait de l'Áeronautique et l'Astronautique, No. 34, Paper. 1972-2
- Yeh Y and Cummins H.Z., Localized Fluid Flow Measurements with a He-Ne Laser Spectrometer, Appl. Phys. Lett., 4, pp. 176-178, 1964

13. LIST OF FIGURES

<i>Figure 1: Flow Visualization around the Sting in Lab</i>	8
<i>Figure 2: Fringe Pattern obtained by the interference of two coherent laser beams and the resulting intensity distribution</i>	11
<i>Figure 3: Schematic of the water tunnel</i>	12
<i>Figure 4: Drag Coefficient for a smooth cylinder as a function of Reynolds number</i>	13
<i>Figure 5: Isometric view of the assembly</i>	14
<i>Figure 6: Sectional view of the L Plate</i>	15
<i>Figure 7: Sectional view of the struts</i>	16
<i>Figure 8: Sectional view of the cylinder</i>	17
<i>Figure 9: Mechanical characteristics of the Angle Plate</i>	18
<i>Figure 10: Mechanical characteristics of the Spacer Block</i>	18
<i>Figure 11: Mechanical characteristics of the Strut</i>	18
<i>Figure 12: Mechanical characteristics of the Cylinder</i>	19
<i>Figure 13: Mesh characteristics</i>	19
<i>Figure 14: Von Mises Stress</i>	22
<i>Figure 15: Displacements in the Strut</i>	23
<i>Figure 16: Variation in the peak frequency as a function of the chosen signal length in ms</i>	25
<i>Figure 17: Power Spectrum of the 20s signal, in the free stream at 3in/s</i>	26
<i>Figure 18: Power Spectrum of the 20s signal, in the wake at z=0 for Re=2962</i>	26
<i>Figure 19: LDV calibration</i>	28
<i>Figure 20: Schematic of the parameter used to determine the separation point</i>	29
<i>Figure 21: Visualization with no flow in the tunnel</i>	30
<i>Figure 22: Instantaneous magnified image of the simulated flow domain indicating the presence of the confluence point in the wake after 260 time steps</i>	31
<i>Figure 23: Instantaneous magnified image of the simulated flow domain indicating the flow path superimposed on the velocity contours of the unsteady flow solution</i>	31
<i>Figure 24: Free shear layer and delayed eddy curl up in the shear layer at Re of 900</i>	33
<i>Figure 25: Formation of the confluence point and the free shear layer with the arrows indicating the entrainment of the free stream between the shed eddies at Re of 900</i>	33

<i>Figure 26: Flow at $Re=5400$, the eddy formation distance is much shorter when compared to the flow at $Re=900$</i>	<i>35</i>
<i>Figure 27: Flow at $Re=9000$, showing a large separation angle, indicating early separation along with turbulence in the wake</i>	<i>36</i>
<i>Figure 28: Frequency distribution of each truncated signal at a flow speed of 4 in/s</i>	<i>36</i>
<i>Figure 29: Comparison of measured frequency distribution with the Gaussian distribution</i>	<i>38</i>
<i>Figure 30: Sample frequency distribution in the wake at a distance of 5D</i>	<i>38</i>
<i>Figure 31: Sample frequency distribution in the wake at a distance of 7.5D</i>	<i>39</i>
<i>Figure 32: Mean wake profile at 7.5D behind the cylinder measured using the LDV</i>	<i>40</i>
<i>Figure 33: Mean wake profile at 7.5D measured using the hot wire</i>	<i>40</i>
<i>Figure 34: Fluctuations in the free stream for a flow speed of 3 in/s (Raw Signal)</i>	<i>42</i>
<i>Figure 35: Fluctuations in the free stream for a flow speed of 3 in/s (Smooth Signal)</i>	<i>43</i>
<i>Figure 36: Fluctuations in the free stream for different flow speeds</i>	<i>43</i>
<i>Figure 37: Fluctuations in the free Stream as a function of the flow speed</i>	<i>44</i>
<i>Figure 38: Fluctuations downstream at $x=7.5D$, $y=0$, $z=0$ and $Re=5100$</i>	<i>45</i>
<i>Figure 39: Fluctuations in the wake at $x=7.5D$, $y=0$, $z=0$ $Re=5100$, averaged every 2 points</i>	<i>45</i>
<i>Figure 40: Power spectrum of the signal shown on Figure 39</i>	<i>46</i>

14. LIST OF TABLES

<i>Table 1: Flow Regimes</i>	7
<i>Table 2: Description of each of the Parts for the Setup along with the Required Quantity</i>	17
<i>Table 3: Summary of Predicted trend in Separation and Eddy Formation distance in the Free Shear based on Image Processing</i>	35
<i>Table 4: Comparison of the measured Coefficient of Drag using the LDV and the Hot Wire techniques in the Water Tunnel and Wind Tunnel Respectively</i>	41

MATLAB SCRIPT

```
clear all
clc
close all
[X_uncut,t_uncut]=tekread('3in_per_sec.wfm'); %Read the signal from the scope
figure(1)
plot(t_uncut,X_uncut) %Plot the signal from the scope to check if we have the right signal

%Sampling Frequency (s-1)chosen when using the scope
Fs = 100e3;

%time step (s) corresponding to the length of a cut signal
time_step=60e-3;

%number of subdivisions
n=floor((t_uncut(length(t_uncut))-t_uncut(1))/time_step);

%Length of uncut signal
L_uncut=length(X_uncut);

%Length of each cut signal
L_cut=floor(L_uncut/n);

for i=1:n
% Cut the signal
    x=X_uncut(1+L_cut*(i-1):L_cut*i);
    t=t_uncut(1+L_cut*(i-1):L_cut*i);

% Use next highest power of 2 greater than or equal to length(x) to calculate FFT.
    nfft= 2^(nextpow2(length(x)));

% Take fft, padding with zeros so that length(fftx) is equal to nfft
    fftx = fft(x,nfft);

% Calculate the number of unique points
    NumUniquePts = ceil((nfft+1)/2);

% FFT is symmetric, throw away second half
    fftx = fftx(1:NumUniquePts);

% Take the magnitude of fft of x and scale the fft so that it is not a function of % the length of x
    mx = abs(fftx)/length(x);

% Take the square of the magnitude of fft of x.
    mx = mx.^2;

% Since we dropped half the FFT, we multiply mx by 2 to keep the same energy.
% The DC component and Nyquist component, if it exists, are unique and should not
% be multiplied by 2.

if rem(nfft, 2) % odd nfft excludes Nyquist point
    mx(2:end) = mx(2:end)*2;
else
```

```

mx(2:end -1) = mx(2:end -1)*2;
end

% This is an evenly spaced frequency vector with NumUniquePts points.
f = (1e-3)*(0:NumUniquePts-1)*Fs/nfft;
% Select a range of frequencies for the Power Spectrum Analysis
for j=1:length(f)
    if f(j)<6
        Bmin=j;
    else if f(j)>8
        Bmax=j;
        break;
    end
end
end
end

% Generate the plot, title and labels if needed.
figure(i)
% semilogy(f(Bmin:Bmax),mx(Bmin: Bmax));
%title('Power Spectrum of the signal ');
%xlabel('Frequency (kHz) ');
%ylabel('Power');
%hold on;

%Search for the highest peak
index=find(mx==max(mx(Bmin: Bmax)));

% mainFreqStr=num2str(f(index));
% plot(f(index),mx(index),'r.', 'MarkerSize',25);
% text(f(index),mx(index),['Frequency = ',mainFreqStr,' kHz ']);
%hold off;
%end

%Vector F contains the frequencies and T the time
F(i)=f(index);
T(i)=t(index);
end

%Plot the fluctuations as a function of time
figure(2)
plot(T,F,'b')
title('Fluctuations');
xlabel('time (s) ');
ylabel('Particles Frequency (kHz) ');

%Output the mean of the signal
mean(F)

%Smooth the signal out
Fa=[];
Ta=[];
%Lcut corresponds to the number of points that we want to average
Lcut=15;
Nd=length(F)/Lcut;
for i=1:Nd
    Fav=sum(F((i-1)*Lcut+1:i*Lcut))/Lcut;
    Tav=sum(T((i-1)*Lcut+1:i*Lcut))/Lcut;
end

```

```

Fa=[Fa;Fav];
Ta=[Ta;Tav];
end
%Faa is the smooth signal centered on the x-axis and giving the result as a
%percentage of deviation from the mean
Faa=((Fa-mean(Fa))/mean(Fa))*100;
%Plot Faa
figure(3)
plot(Ta,Faa,'k - o')
title('Averaged Fluctuations');
xlabel('time (s) ');
ylabel('Fluctuations around the mean / mean (%) ');
legend('3in/s')

```

%Power Spectrum Analysis of F (same method as before)

```

%Sampling Frequency
Fsa=length(F)/(T(length(T))-T(1));
nfft2= 2^(nextpow2(length(F)));
fftF = fft(F,nfft2);
NumUniquePts2 = ceil((nfft2+1)/2);
fftF = fftF(1:NumUniquePts2);
mF = abs(fftF)/length(F);
mF = mF.^2;
if rem(nfft2, 2)
    mF(2:end) = mF(2:end)*2;
else
    mF(2:end -1) = mF(2:end -1)*2;
end
f2 = (0:NumUniquePts2-1)*Fsa/nfft2;
for j=1:length(f2)
    if f2(j)<0.1
        Cmin=j;
    end
end
% Generate the plot, title and labels.
figure(4)
semilogy(f2(Cmin:length(f2)),mF(Cmin:length(mF)));
title('Power Spectrum of the signal');
xlabel('Frequency (Hz)');
ylabel('Power');
hold on;
index2=find(mF==max(mF(Cmin:length(mF)))));
mainFreqStr2=num2str(f2(index2));
plot(f2(index2),mF(index2),'r.', 'MarkerSize',25);
text(f2(index2),mF(index2),['Frequency = ',mainFreqStr2]);
hold off;

```

RESPONSE TO COMMENTS

Dear Sir,

We gratefully acknowledge the suggestions provided based on the presentation of the project and hope that the following discussion answers the questions appropriately.

- *“Please find the Strouhal number for the near-periodic wake fluctuations and compare to the air tunnel data”*

We have mentioned in our report that the eddy shedding frequency was 0.8 Hz for a flow speed of 5.1 in/s. The eddy shedding frequency was obtained from a video capture of the flow. This gives us a Strouhal number of 0.24. Unfortunately this was not a parameter which we compared with the measurements from the wind tunnel. However, we have approached another group which had done an analysis on the vortex shedding frequency in the wind tunnel and the following are the results:

For a flow speed of 3.07 m/s, the vortex shedding frequency was found to be 66 Hz and for a flow speed of 3.97 m/s, the vortex shedding frequency was found to be 87 Hz. Both of these give a Strouhal number of 0.27.

One would expect the Strouhal number in this flow regime (transition in the shear layer, $Re = 800-20000$) to remain constant. The effect of shortening of the near wake is accompanied by the widening of the turbulent shear layer, thus each of them nullifying the effect of the other, maintaining a constant Strouhal number.

- *“What do you mean by the 'angle at which the shear layer departs'?”*

A discussion on this has been included in the section on the Results and Discussion, page 28-29, under the sub section on Flow Visualization.

Sincerely,

Arnab Ganguly and Jeremy Nabeth